

can be understood as follows. The triangular and square lattice tilings require that its constituents be edge-to-edge. From an entropic standpoint, there are an infinite number of tilings by arbitrarily translating rows or columns of triangles and squares. The self-assembly of edge-edge ATs at finite density implies that there is a free energy difference between aligned and misaligned states. Free energy calculations were performed to quantify the effect of alignment on the free energy. The effect of density and shape were explored (Figures 3.6a,b). For dense fluids of hard triangles (Figure 3.6a,b), there is a free energy difference between the aligned and misaligned state of $1.2k_B T$. Above and near the crystallization packing fraction ($\rho=0.75$) the free energy difference increases to $2.5k_B T$. The increase in free energy at high packing fraction penalizes misalignments and drives the system to the (3^6) AT. On the other hand, the degree of faceting has an inverse effect on the free energy. As the number of facets increases, a polygon behaves more like a disk. Indeed we observe that the directional entropic forces lose directionality for increased faceting. Directional entropic forces weaken considerably with the number of facets since they arise from a drive toward dense local packing, and the local packing becomes less dense as the number of facets increases. *van Anders et al.* (2013a) For example, the hard triangle has an entropic penalty of $2.5k_B T$ for misalignment, whereas at the same density the dodecagon has an entropic penalty of only $0.3k_B T$. For the ATs with degenerate ground states, such as the (3^6) and (4^4) ATs, directional entropic forces explain the preferential edge-edge alignment of the assemblies. They also explain the thermodynamic stability of the (3.12^3) and (6^3) Archimedean tiling at finite packing fractions. As a final note, we observed that the inclusion of attractive patchy interactions does not inhibit the formation of any of these four ATs.

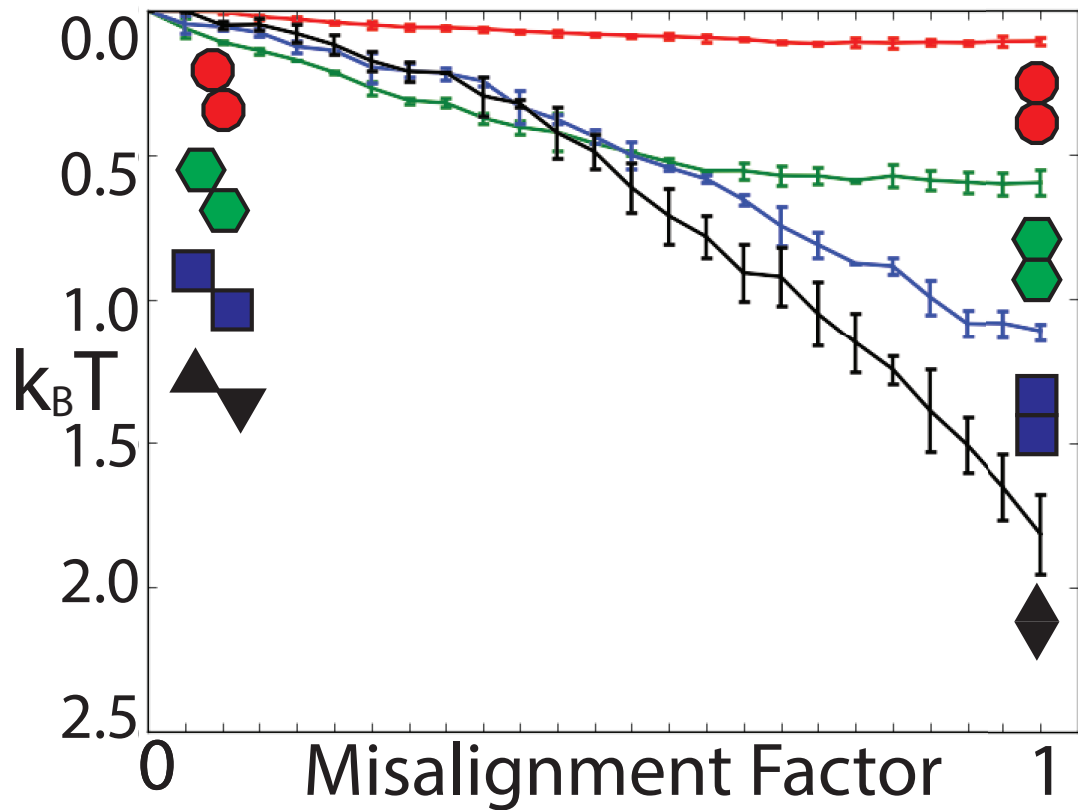


Figure 3.6: . Effect of shape on the effective free energy difference at fixed density. The blue line overlaid on top of the triangles shows the free energy gain by aligning the edges of the shapes. We show the free energy difference as a function of the misalignment factor f . The free energy gain for edge-edge alignment is $2.5k_B T$ for triangles, $1.1k_B T$ for square, $0.6k_B T$ for hexagons, and $0.2k_B T$ for dodecagons.

3.5.2 Symmetric Enthalpic Interactions

We find that entropy alone is insufficient to assemble the remaining ATs, and enthalpic interactions must be included. In these cases, enthalpy biases the free energy to promote edge-edge binding, and can stabilize open structures that would not be possible with purely entropic forces.

Like the (3.12^3) AT, the (4.8^2) AT can be most easily assembled using only octagons, and treating the square tiles as pores. However, because hard octagons favor a hexagonal crystal structure (Figure 3.7a), attraction between nanoplate edges is required to stabilize the AT. The hexagonal crystal structure has misaligned edge-edge bonds with an entropic penalty of $0.5k_B T$ per edge at $\rho \geq 0.8$. The two barriers to entropic self-assembly of the (4.8^2) AT with hard octagons are packing constraints and the coordination of this semi-regular tiling. At $\rho 0.8284$, the (4.8^2) AT cannot self-assemble due to particle overlaps. At lower packing fractions, the free energy penalty for misalignment is $0.2 k_B T$. Two-thirds of the edge-edge octagons are 50% misaligned, while the remaining bonds are aligned in the hexagonal crystal structure. The hexagonal crystal structure exhibits a higher coordination (6 nearest neighbor bonds) as compared to the truncated square AT (4 nearest neighbor bonds), which compensates for the entropic penalty due to misalignments. The partial misalignments of the hexagonal crystal structure are entropically favored to the aligned edge-edge bonds of the (4.8^2) Archimedean tiling due to the effect of coordination and packing constraints. In simple terms, the ideal (4.8^2) Archimedean crystalline structure with regular octagons has a packing fraction of 0.8284. This value is below the maximum packing fraction of hard regular octagons, which tend to form the hexagonal structure. Consequently, we anticipate attractive interactions are needed to stabilize the (4.8^2) AT. Indeed, by adding short-ranged attractive patches of strength to each edge of the octagon, we find the (4.8^2) AT robustly self-assembles (Figure 7b). Binary mixtures of octagons and squares with attractive patches also form this

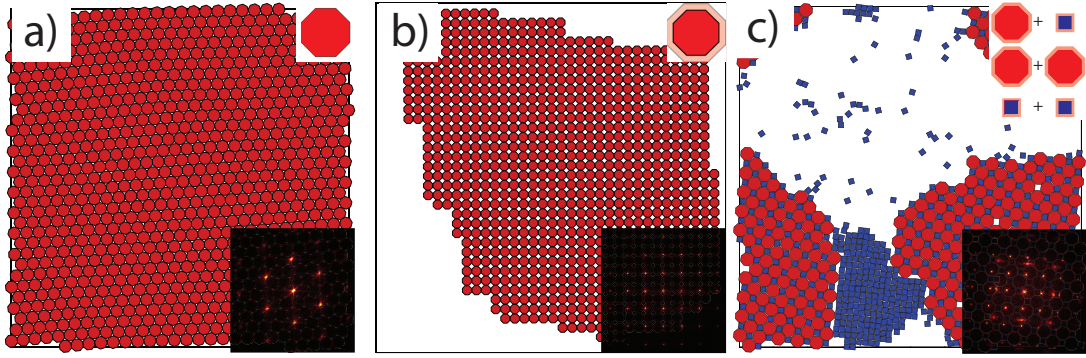


Figure 3.7: Hard vs. symmetrically attractive octagons. (a) Hard octagons (upper-right inset) assemble into a hexagonal crystal structure. (b) Symmetrically attractive octagons (upper-right inset) form the defect-free (4.8^2) AT where the squares are treated as pores. Both snapshots are accompanied by a diffraction pattern showing long-range order. (c) Truncated square tiling formed from octagons and squares with symmetric attractive interactions in a 1:2 mixture ratio. Excess squares formed the (4^4) square tiling upon further annealing.

semiregular AT (Figure 3.7c). It is interesting to note that the AT forms without the perfect stoichiometric ratio of tiles. The excess squares form the (4^4) AT. This result is important because experiments will not be constrained by stoichiometry in seeking the (4.8^2) AT. (Figure 3.7c)

3.5.3 Shape Specific Enthalpic Interactions

The five ATs studied thus far were each assembled using a single tile shape, even when multiple tiles technically comprise the tiling and one of the tile shapes is considered a pore. The remaining six ATs all require a minimum of two tile shapes. Of these, three $(3^2.4.3.4)$, $(3.4.6.4)$ and $(3.6.3.6)$ require shape-specific interactions (Figure 3.8b,d, and f, respectively). As defined previously, shape specificity implies that the interaction between dissimilar rather than similar - species is favored, an asymmetry recently observed in rod-sphere shape alloys. *Ye et al. (2013a)*

The two insets of each panel in Figure 8 highlight the matching rules between polygons and the corresponding diffraction pattern of the assembly. The matching

rules show all combinations of building blocks and the strength of each edge-edge interaction for all interaction pairs. The interaction strength (ϵ) is visualized by the color of the halo around the building block, where red is weak and green is strong. The strength of the strong interaction depends on the targeted AT, as discussed below.

Binary mixtures of symmetric attractive polygons demix or form disordered aggregates. Square-triangle mixtures with symmetric interactions tend to be disordered at intermediate densities because the difference in the free energies of the demixed (pure square and pure triangle) phase vs. the mixed phase is small (Figure 3.8a). In contrast, hexagon-square and hexagon-triangle mixtures with symmetric interactions demix at intermediate densities (Figure 3.8c,e). Symmetrically attractive mixtures of regular hexagons and triangles using the stoichiometry of the (3.6.3.6) AT demix and form, as coexisting phases, the 3^6 and 6^3 ATs. Similarly, symmetrically attractive mixtures of the rhombitrihexagonal (3.4.6.4) AT demix into pure hexagonal and square ATs (Figure 3.8c,e). This natural trend to demixing is also observed in mixtures of hard polygons of the same shapes. In the presence of symmetric attractions, we observe a hierarchy of freezing temperatures. Below but close to the first freezing temperature, the polygons with the most edges crystallize first since these polygons possess more enthalpic bonds (higher crystal coordination), while the less faceted polygons remain in a liquid phase. Further cooling to the second freezing temperature leads to the crystallization of the smaller polygons. As the difference in the number of enthalpic edges of both particles increases, so does the separation between these two freezing temperatures. Thus for square-triangle mixtures the difference is small leading to disorder. For triangle-hexagon and square-hexagon mixtures the difference between melting temperatures increases ($(T_1 - T_2)/T_1 \sim 0.2$, where T_1 and T_2 are the first and second freezing temperatures), leading to complete bulk demixing. By biasing the opposite shape interaction (hexagon-triangle, square-triangle, hexagon-square) using shape-specific interactions, the ($3^2.4.3.4$), (3.6.3.6), and (3.4.6.4) ATs

will self-assemble (Figure 3.8b,d,f). The (3.4.6.4) tiling was self-assembled as a binary mixture because the ternary mixtures matching rules are more complex. A pore acts as the triangle tile in this patchy polygon design. The minimum asymmetry in the interaction strength to self-assemble the (3².4.3.4), (3.6.3.6), (3.4.6.4) ATs are 1.2 ϵ , 1.5 ϵ and 1.2 ϵ , respectively.

3.5.4 Edge-Specific Enthalpic Interactions

In the previous section, shape-specific interaction of triangle-square, hexagon-square, and hexagon-triangle shape alloys were shown to self-assemble the (3².4.3.4), (3.4.6.4), (3.6.3.6) ATs. The mixtures that self-assemble the (3².4.3.4), (3.4.6.4), (3.6.3.6) ATs have similar mixing ratio as the (3³.4²), (3⁴.6), (4.6.12) ATs. The mixing ratio for the (3⁴.6) AT (triangle-to-hexagon 8:1) is greater than that of the (3.6.3.6) tiling. For a triangle-to-hexagon 8:1 mixture ratio, we observe coexistence between the (3.6.3.6) tiling and a triangular tiling formed by excess triangles (Figure 3.8e). The demixing observed between excess triangles and the self-assembled (3.6.3.6) AT is similar to that observed between excess squares and the (4.8²) AT. As shown before, shape-specific interactions for these mixtures self-assemble the (3².4.3.4), (3.4.6.4) and (3.6.3.6) ATs (Figure 3.8 a,c and e).

Edge specific patchy interactions increase the interaction specificity. As previously mentioned (Model and Approach Section), edge-specific interactions are a type of interaction in which each edge pair can have unique interaction strength ij , where i and j correspond to edge indices on different building blocks. Edge-specific interactions allow the self-assembly of complex crystalline structures, and occur naturally in crystalline nanoplates due to energetic differences between different crystallographic edges. *Ye et al.* (2013c)

The minimal designs of the (3³.4²), (4.6.12) and (3⁴.6) AT are shown in Figure 3.9.b,d and f. In the case of the elongated triangular AT, self-assembly requires

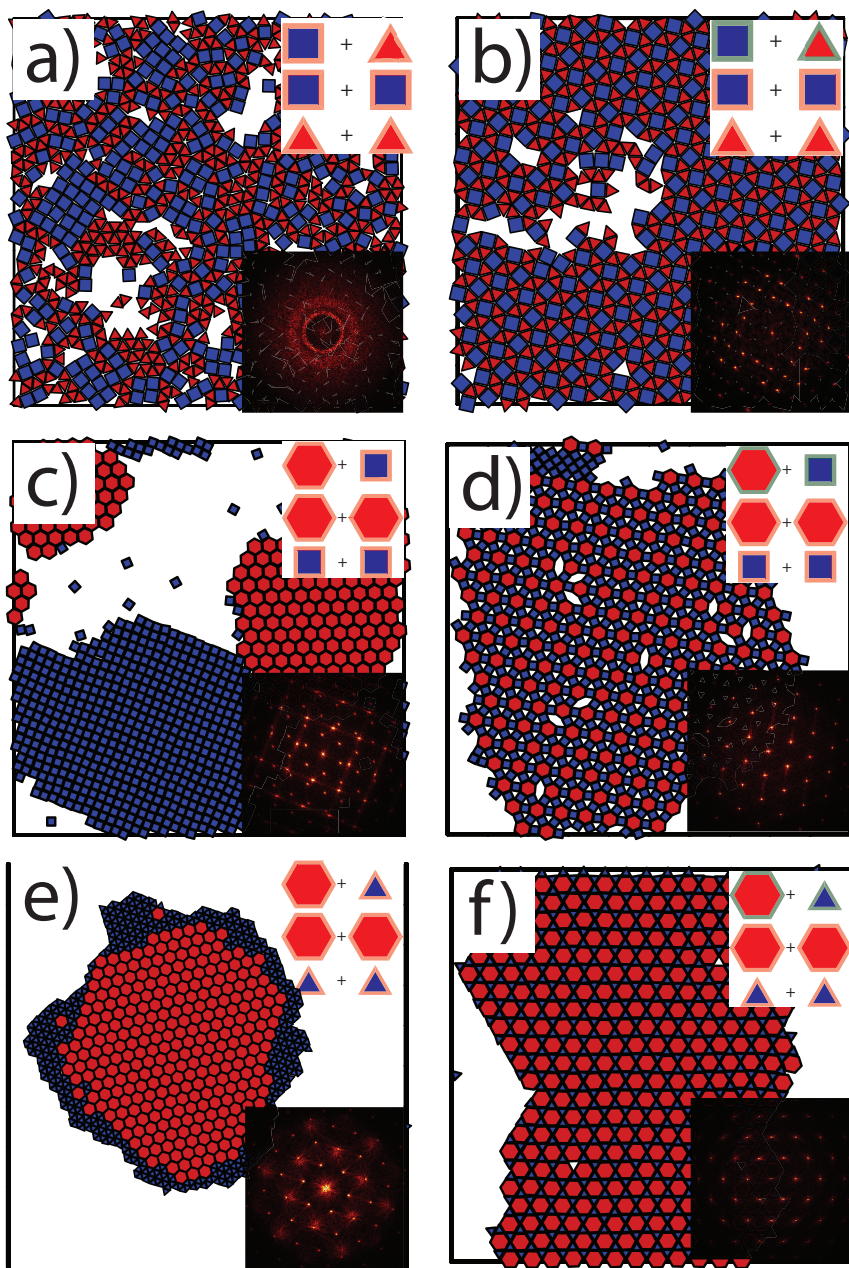


Figure 3.8: Representative snapshots of the design process for the $(3^2.4.3.4)$, $(3.4.6.4)$, and $(3.6.3.6)$ ATs. Insets show the design rules and a diffraction pattern. A red halo implies a weakly attractive interaction, while a green halo implies a strong attractive interaction. Left column panels shows symmetrically-attractive mixtures of (a) square-triangle, (c) square-hexagon and (e) triangle-hexagon mixtures. Right column panels correspond to the mixtures in the left column with shape-specific patches that readily self-assembles (b) the $(3^2.4.3.4)$, (d) $(3.4.6.4)$, and (f) $(3.6.3.6)$ ATs

strong attraction between opposite edges of the square and one edge of the triangle, and a stronger attraction between the edges that do not attract triangles. The edge pair of the triangles that do not attach preferentially to squares interact strongly. The assembly in Figure 3.9b requires a strong interaction asymmetry of $\sigma = 1.2\epsilon$ (green edges). The design biases energetically the unit cells of the (3^3) AT. The minimal design for the $(4.6.12)$ Archimedean tiling requires strong attraction ($\sigma = 1.25\epsilon$) between alternating edges of hexagon and squares. The remaining edges of both shapes are weakly attractive (inset in Figure 3.9d). Hexagons and squares form rings, which is consistent with the truncated hexagonal AT. The assembly is not free of defects, and in some cases single or multiple polygons are encircled by these rings (Figure 3.9d).

In the minimal design for the $(3^4.6)$ Archimedean tiling, all edges of the hexagon preferentially attach to one specific edge on the triangles, the hexagon-to-hexagon edge attraction is weak ($\sigma = 1\epsilon$), and triangles preferentially attach to each other on edges that do not preferentially attract hexagon edges (Figure 3.9f). By making the hexagon preferentially attractive to one side of the triangle, all edges of the hexagon become saturated and the triangle-triangle interaction completes the tiling. For the assembly in Figure 3.9f, the interaction asymmetry σ is 3ϵ . Due to the complexity of this set of design rules, multiple point defects are observed. This AT is chiral, however no bias towards either handedness was observed. Thus, to form the snub hexagonal AT with a targeted chirality, further complexity in polygon patchiness is needed.

3.6 Discussion

We approached the design of nanoplates to assemble the Archimedean tilings by ascertaining the simplest set of interactions yielding the desired tiling. The multistep design process summarized on the left-hand side in Figure 3.4 uses information about the target tiling and building block. We first minimize the number of building blocks

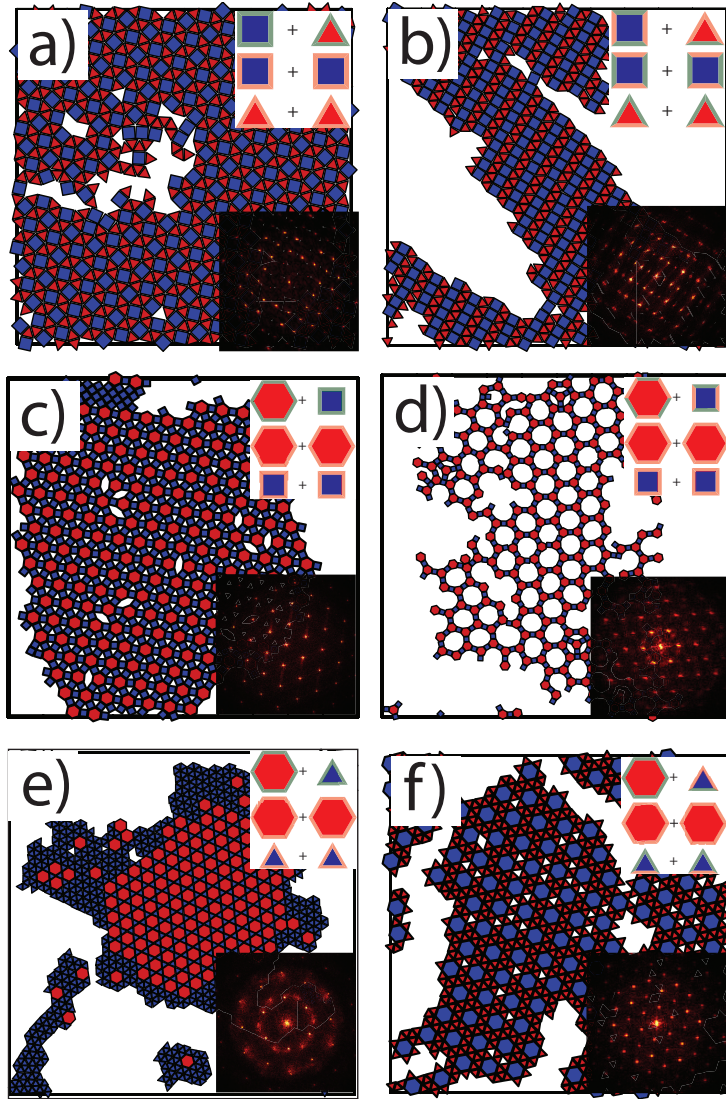


Figure 3.9: Representative snapshots for the design process of the $(3^3.4^2)$, $(3^4.6)$ and $(4.6.12)$ Archimedean tilings. Each panel is accompanied by an inset showing the design rules for assembly and a diffraction pattern confirming long-range order or coexistence. The mixture ratio for each assembly corresponds to that of the target AT. A red halo around a polygon implies a weaker attractive interaction, while a green halo implies a stronger attraction. Left column panels show shape-specific attractive triangle-square, hexagon-square and triangle-hexagon mixtures that self-assemble the (a) $(3^2.4.3.4)$, (c) $(3.4.6.4)$ and (e) $(3.6.3.6)$ ATs. Residual triangles form the (3^6) AT in (e). Right column panels show shape-specific attractive triangle-square, hexagon-square and triangle-hexagon mixtures that self-assemble the (b) $(3^3.4^2)$ tiling, (d) $(4.6.12)$ and (f) $(3^4.6)$ ATs, respectively.

to self-assemble the targeted tiling. For the (3.12^2) , (4.8^2) , $(3.4.6.4)$ and $(4.6.12)$ AT, one of the polygonal tiles is replaced by a pore, and the resulting tiling no longer fills space, but is instead open and porous.

After selecting the building blocks, the design process examined the constituent polygonal building blocks, and alters the interaction complexity by changing the specificity of interactions. The four models ranked in terms of specificity are hard, symmetric patches, shape-specific patches and edge-specific patches. Our design process reveals why for each AT a certain degree of specificity is needed for self-assembly. Initially, we test if entropic interactions are sufficient to self-assemble each crystalline structure. If the infinite pressure ground state is not the candidate crystal structure, we find attractive interactions are needed to self-assemble the crystalline structure. (Figure 3.4) Due to the highly symmetric polygons used to self-assemble the ATs, we argue that an effective entropic edge-edge interaction will stabilize these highly symmetric groundstates. For crystal structures with one building block that are not the infinite pressure ground state, symmetric attractive patches are sufficient for assembly (Figure 3.4). For mixtures of building blocks, the complexity of the crystal structure determines the complexity of the interaction potential. Hard (entropic) mixtures show a natural trend to partial demixing and do not form crystalline monolayers with discrete symmetries. Symmetric attractive mixtures also demix, with no indicative behavior towards the formation of binary ATs at intermediate densities. We posit that the hard mixtures segregate due to a depletion effect. *Dijkstra et al.* (1999) Since hard and symmetrically attractive building blocks demix, selective patchiness must be used to overcome this natural trend (Figure 3.4). The local environment for each polygonal tile in the target AT determines the arrangement of patches. If an alternating building block crystal structure is present, shape specific patches are sufficient to design the crystalline structure (Figure 3.4). An alternate building block structure is a binary mixture in which the large polygonal tile is surrounded by the

small tile, and the small tile has at most one bond with another small tile. If the crystalline structure for a mixture of building blocks does not contain the alternating building block property, it is necessary to use edge specific interactions. The assembly complexity of the building block and crystal structure provides the necessary information to self-assemble the AT.

The description of minimal design rules for self-assembly is related to tiling models in computer science and mathematical descriptions of graph connectivity. The general complexity of edge connectivity problems is known to be NP hard *Demaine and Demaine* (2007), which weakens the attractiveness of an algorithmic approach to the development of design rules for crystal structures. Mathematical work on the edge coloring of Archimedean graphs *Fjærestad* (2010) does not provide sufficient information to develop design rules for self-assembly. In effect, an iterative, heuristic approach as described in this paper is the best one can do to develop design rules for self-assembly of tilings such as these.

3.7 Conclusion

Ascertaining assembly complexity is an essential feature of our design strategy for mixtures of anisotropic patchy particles. We ranked each AT from (3⁶) to the (4.6.12) in order of assembly complexity. Self-assembly complexity is the complexity of the simplest set of interactions and building blocks that self-assemble the candidate crystal structure with a minimal number of crystallographic defects. (Figure 3.4) We described the design strategy in a flow diagram (Figure 4). The flow diagram describes the steps used to design the interactions of the building blocks. To the right of the design flow diagram, we overview material systems *Chu et al.* (2006); *An et al.* (2007); *Xiong et al.* (2005); *Li et al.* (2009b); *Guo et al.* (2012); *Zhou et al.* (2008); *Xu et al.* (2006); *Wang et al.* (2010); *Zhang and Zhu* (2005); *Su et al.* (2010); *Cao* (2004); *Park et al.* (2011); *Xi and Ye* (2010); *Paik et al.* (2013); *Kan et al.*

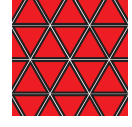
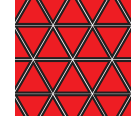
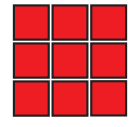
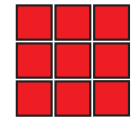
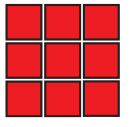
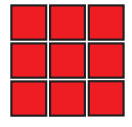
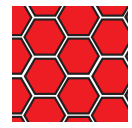
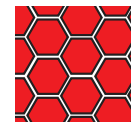
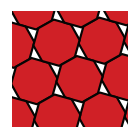
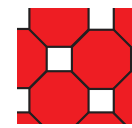
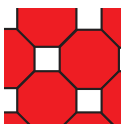
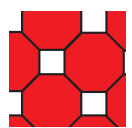
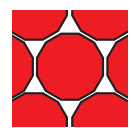
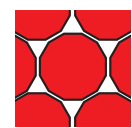
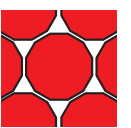
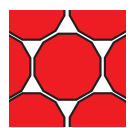
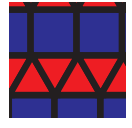
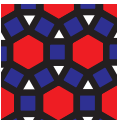
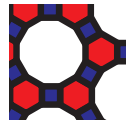
	Hard	Attraction	Shape Specific Patches	Edge Specific Patches
				
				
				
				
				
	Disordered	Disordered		
	Disordered	Demixing  + 		
	Disordered	Demixing  + 		

Figure 3.10: Simulation results summary. The first column shows the polygons necessary for the assembly of ATs under the design rules proposed. The remaining columns indicate the configurations observed with the different interaction sets..

(2010); *Zeng et al.* (2010) that can form the anisotropic nanoplates consistent with the ATs, and material systems that self-assemble *Sau and Murphy* (2005); *Lee et al.* (2006); *Park et al.* (2006); *Li et al.* (2010); *Ye et al.* (2010); *Shen et al.* (2012b); *Sun and Xia* (2002); *Chen et al.* (2007b); *Paik et al.* (2011); *Zhang et al.* (2005a) ATs with nanoplates (Fig 3.2) The regular entropically stabilized $(3^6),(4^4),(6^3)$ ATs have been observed experimentally with polygonal tiles, but the other Archimedean tilings remain elusive (Figs 3.2 and 3.4). Furthermore, nanoplates covered with DNA, although not experimentally synthesized, is a natural evolution of DNA grafting on nanomaterials. *Nykypanchuk et al.* (2008); *Maye et al.* (2010) Such DNA tiles provide another means for achieving the necessary interaction specificity to assemble ATs

The building block design process offers insight into the necessary conditions to self-assemble crystals with regular polygons (nanoplates). The design process has led to important conclusions about shape and self-assembly, summarized in Figure 3.10. With only entropy, certain Archimedean tilings can self-assemble their infinite pressure packings at intermediate packing fractions. This finding reinforces the perspective on an entropic patch as a driver for self-assembly. *van Anders et al.* (2013a) On the other hand, for low density packings symmetric enthalpic patches are required. Binary mixtures of regular shapes have a rich behavior that depends on the type of interactions and geometry. We observe that hard binary mixtures tend to be disordered when mixed. By adding enthalpic patches, demixing occurs if the difference between the coordination of the polygons is large. This is confirmed by hexagon-square and hexagon-triangle assemblies demixing, whereas square-triangle mixtures are disordered. Shape-specific and edge-specific patches stabilize the remaining semi-regular tilings. Although nanoplate patterning inspires the designs developed in this work, these enthalpic design rules can also be expanded to supramolecular systems, where particle interactions are programmable and system dynamics are faster.

CHAPTER IV

The Effect of Geometric Transformations on the Self-assembly Properties of Faceted Nanoplates

4.1 Abstract

The geometry of different nanomaterials provides a means of driving self-assembly into a myriad of crystal structures *Damasceno et al. (2012a)*. As the shape control of different nanomaterials improves *Xia et al. (2009a)*, design frameworks *Glotzer and Solomon (2007)* become necessary to understand the collective properties of different classes of materials from the surface functionalization and geometry of building blocks. Here, we study the self-assembly of polygonal nanoplates with attractive short-range forces via Monte Carlo simulations. We investigate the effect of geometric transformations such as elongation and faceting on the assembly on ligand-stabilized nanoplates. We report the effect of each experimentally feasible geometric transformations on the assembly and, from this information, develop design rules to assemble complex structures

4.2 Introduction

Shape is a promising route towards the assembly of complex crystal structures. Anisotropic nanoparticles can robustly self-assemble complex crystal structures *Dam-*

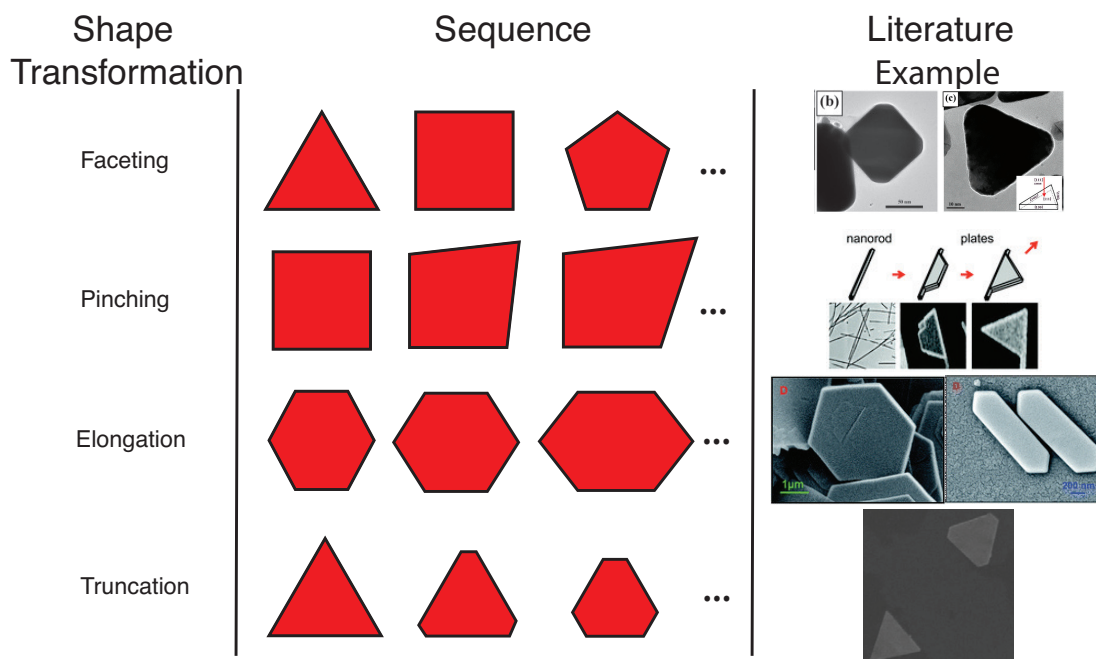


Figure 4.1: Examples of shape transformations for nanoplates. The first column corresponds to the classification of experimentally-observed shape transformations. These shape transformations correspond to faceting, pinching, elongation, and truncation. The second column depicts the effect of the transformation on particle shape. Experimental examples of the shape transformation are shown in the third column. The faceting shape transformation is shown for silver nanoplates. *Yang et al.* (2007) The pinch transformation is shown for the growth of a silver triangular nanoplates on a nanorod. *Tsuji et al.* (2010) The elongation transformation is shown for uranium oxide hydroxide hexagonal nanoplates. *Pradhan et al.* (2011) The truncation transformation is shown for hexagonal and triangular nanoplates. *Chu et al.* (2006)

asceno et al. (2012a) with interesting catalytic *Narayanan and El-Sayed* (2005) and plasmonic *Wiley et al.* (2006b) properties. Folded nanoparticles *Leong et al.* (2007a) and 3D printers *Mannoor et al.* (2013) have the potential to drastically increase the type of particle shapes that can be self-assembled. As the size and scope of the nanoscale self-assembly field grows, rational design rules become paramount to the future prospects of synthesizing novel materials with promising photonic *Jensen and Sigmund* (2011), plasmonic *Viarbitskaya et al.* (2013), and mechanical *Kohlstedt and Glotzer* (2013) properties.

Shape optimization is a form of optimal control theory, which finds the optimal shape that minimizes a certain cost functional with well-defined constraints. *Sokolowski and Zolesio* (1992) Shape optimization has been used to optimize fluids *Mohammadi and Pironneau* (2004), aircraft wings *Sobieszcanski-Sobieski and Haftka* (1997) , and to improve the mechanical properties of skeletal structures such as trusses *Topping* (1983). On the micro and nanoscale, shape optimization has been used to design waveguides and resonators for nanophotonics *Jensen and Sigmund* (2011), to design micromixers *Ansari and Kim* (2007) , and to improve the gelation properties of colloids *Smrdel et al.* (2008) . The broad spectrum of shape optimization applications begs that shape optimization be used to design faceted shapes for self-assembly.

Shape transformations can be active (in situ) or passive transformation between two different shapes. Figure 1 shows the experimental manifestations of these transformations. We focus on faceting, pinching, elongation, and truncation transformations observed in faceted nanoplates. Gold is an excellent example of the faceting transformation since it can form triangular, square, pentagonal, hexagonal, nonagonal, and dodecagonal microplates and nanoplates. *Porel et al.* (2005); *Kan et al.* (2010) (See Figure 4.1) Silver can transform through pinching from a nanorod to a nanorod with a triangular nanoplates (as a nanoflag). *Tsuji et al.* (2010) (See Figure 4.1) Passive elongation transformation is observed in Uranium oxide hydroxide and gold. Uranium oxide hydroxide and gold both can form hexagonal and elongated hexagonal nanoplates. *Pradhan et al.* (2011); *Umar et al.* (2009) (See Figure 1) Gold and silver nanoplates are examples of truncation; gold forms triangular truncated hexagonal and hexagonal nanoplates. *Chu et al.* (2006) and silver nanoplates can actively transforming under light via truncation between triangular and hexagonal nanoplates. *Tang et al.* (2009) (See Figure 4.1) Truncated triangular nanoplates of silver were synthesized in solution coexistent with surfactant micelles. *Chen and Carroll* (2002)

Shape optimization begins with the regular nanoplates. A library of shape transformations must be categorized and understood to guide the optimization procedure. The symmetry-breaking transformation converts the original regular shapes into an irregular polygonal tile with favorable self-assembly properties. The shape transformations alter the directional entropic forces by altering the edge length.*van Anders et al. (2013a)* With the shape transformation library, shape can be optimized to improve the self-assembly properties of a material.

Nanoplates *Cao (2004)*; *Zhang et al. (2005a)*; *Sun and Xia (2003)* have excellent catalytic *Kavan et al. (2011)* , optical *Lu et al. (2006)*, and antibacterial *Pal et al. (2007)* properties. The competition between enthalpic and entropic can lead to rich phase behavior *Ye et al. (2013c)* . Optimized patchy nanoplates have shown to robustly self-assemble the Archimedean tilings.ref Geometric transformations can alter the properties of nanoplates. Truncation can alter the surface plasmon resonance of silver nanomaterials by red-shifting the extinction spectra *Wiley et al. (2006a)*.

Here, we show how to self-assemble polygonal nanoplates into a large number of crystal structures. We investigate the complete family of regular polygons, the n-gons, to understand the role of shape on assembly. We show that the majority of the n-gons self-assemble into Archimedean tilings. The regular pentagon heptagon and nonagon are shown to self-assemble frustrated systems. An iterative shape optimization procedure is used to deform the shape of n-gons to improve the assembly properties of frustrated assemblies and to understand the effect of each transformation on assembly. A design framework is introduced to provide a simplified model of how shape optimization can be used to improve the assembly properties of a faceted nanoparticle.

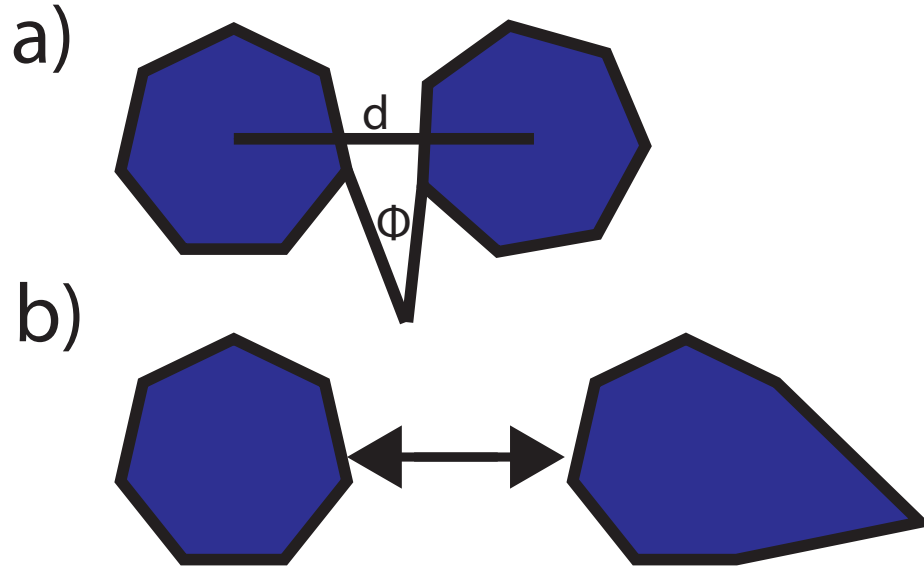


Figure 4.2: Model patchy nanoplates are shown with interactions, and a deformation mechanism. The interactions between the nanoplates is edge to edge(a). The deformation process alters the shape of the nanoplates continuously and reversibly(b).

4.3 Model

We use a phenomenological model for patchy nanoplates. Each particle is modeled as a regular polygon with attractive patches on each edge. The attractive strength is set equal to ϵ for each patch. The edge-edge interaction potential can be decomposed into three components: parallel, perpendicular, and angular components (See Fig. 4.2a). The attractive interaction models the ligand-ligand van der Waals attraction. The perpendicular component captures the strength of the ligand-ligand van der Waals forces, while the parallel and angular components model the steric depletion among ligand-stabilizers. Since ligands are responsible for these attractive interactions, we scale the angular and distance cutoff for the angular and perpendicular component to model the length of the ligands. The angular and perpendicular components scale quadratically with distance and the linear component scales linearly with distance. The attraction is maximized when the edges are aligned, centered, and almost in contact.

4.4 Methods

Particles are represented as ideal polygons, with and without an added short-range interaction. Overlap checks are performed using the GJK algorithm as in *Damasceno et al.* (2012a). The runs are molecular simulations using the Monte Carlo algorithm in the NVT ensemble. In the presence of interactions, pressure and temperature are kept fixed until ordering occurs. System sizes range from 800 to 2000 particles. Simulation times are few millions of Monte Carlo cycles using established simulation codes. *Damasceno et al.* (2012b); *Ye et al.* (2013c)

4.5 Results

The results are divided into the four classes of geometric transformations: faceting, pinching, elongation and shearing. Packing and self-assembly simulations were performed for the n-gon family. We show the effect of each transformation on the self-assembly properties of the deformed n-gon family. We classify the crystalline structures by their center-to-center crystallographic bond network. The results are divided into the faceting, pinching, elongation, and shearing results

4.5.1 Faceting

The faceting transformation alters the number of edges of a regular polygonal nanoplate. It unites all regular polygonal nanoplates into the n-gon family (See Figure 3a). As the number of edges (N) increases, the polygon transforms into a disk. This rounding has a significant effect on the self-assembly at low N . Frustrated assemblies occur at intermediate N for odd number vertices ($N=5,7,9$). Archimedean tilings occur for polygons that have a characteristic Archimedean tiling, such as triangles and the (3^6) Archimedean tiling. The self-assembly results can be divided into three classes: the Archimedean class, the frustrated class, and the disk class.

The faceting transformation provides a continuum between faceted and continuous geometries highlighting the effect of faceting on self-assembly.

In the Archimedean class, the regular polygons self-assemble into a Archimedean tiling. A subset of this class interestingly packs the same as the assembly; the packing of regular polygons is known to form dense periodic packings with quasi 6-fold symmetry. *Duparcmeur* (1995) The packings contact network (edge-vertex, edge-edge) alternates between odd and even number of vertices. *Duparcmeur* (1995) The regular polygons with assemblies in the Archimedean class are the regular triangle, square, hexagon, octagon, and dodecagon; these self-assemble the (3^6) , (4^4) , (6^3) , (4.8^2) , and (3.12^2) Archimedean tilings, respectively (See Figure 4.3a, 4.3b, 4.3e, 4.3k). Previous work on the self-assembly of the Archimedean tilings shows that the (3^6) , (4^4) , (6^3) , and (3.12^2) Archimedean tiling can self-assemble with entropic patches, while the (4.8^2) Archimedean tiling requires enthalpic patches. (See Chapter 4.3)

In the second self-assembly class of the faceting transformation, a crystal does not form. The frustrated class encompasses the regular pentagon, heptagon, and nonagon (See Figure 4.3d, 4.3f, 4.3h). These polygons clearly have five-fold, seven-fold, and nine-fold respectively, symmetry rendering them inconsistent with the standard Bravais lattice coordinations. Theoretical work on the five- and seven-fold coordinated nearest-neighbor rings in assemblies have been shown to cause frustration and inhibit crystallization. *Nelson* (1983) Experimental work on the assembly of five-fold symmetric hydrocarbons has been shown to form a glass. *Merz et al.* (2009) Liquid crystals can form five-fold, seven-fold, and nine-fold quasicrystals. *Gorkhali et al.* (2006) This propensity in nature for five-, seven-, and nine-fold symmetric objects to self-assemble disordered and/or quasicrystalline structures argues for frustration and competition to be prevalent in the assembly of pentagons, heptagons, and nonagons.

For the third self-assembly class, the regular polygon assemblies approximate the disk assembly. Clearly, the more vertices the polygon, has the closer the assembly and

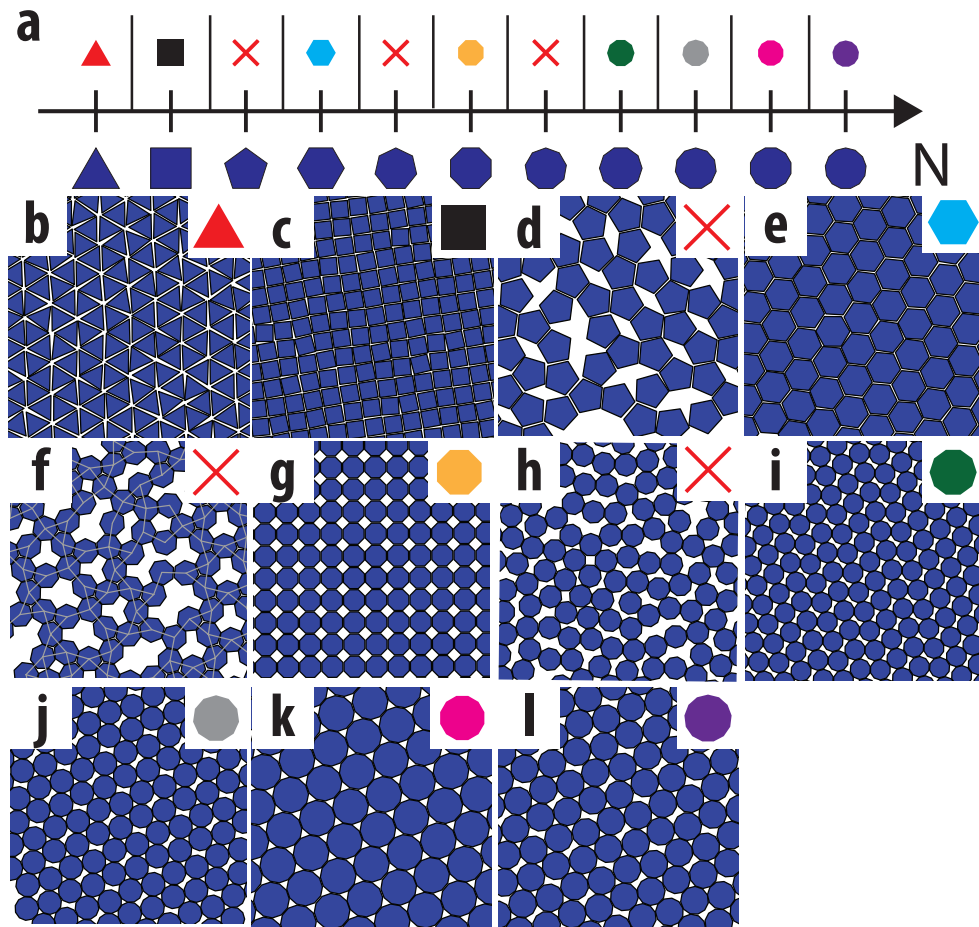


Figure 4.3: The self-assembly of faceted nanoparticles is shown above. The faceting transformation is summarized by a geometric axis showing the regular polygons (a). Red Xs imply a frustrated assembly, while a colored regular polygon denotes assembly. Each snapshot is a representative assembly of the nanoplates. The assemblies for the regular n -gon family are the (3^6) Archimedean tiling for the regular triangle (b), the (4^4) Archimedean tiling for the regular square (c), a frustrated assembly for the regular pentagon (d), the (6^3) Archimedean tiling for the regular hexagon (e), a frustrated assembly for the regular nonagon (f), the (4.8^2) Archimedean tiling for the regular nonagon (g), a frustrated assembly for the regular nonagon (h), a sheared rhombic tiling for the regular decagon (i), a sheared $(3^2.3.4.3)$ Archimedean tiling for the regular undecagon (j), the (3.12^3) Archimedean tiling for the regular dodecagon (k), and a sheared $(3^2.3.4.3)$ Archimedean tiling for the regular hendecagon (l).

shape approximates a disk. At low N , n -gons exhibit a density-driven transition from their assembly to their packing, which approximates disk assembly. For example, a transformation between the (4.8^2) Archimedean tiling and the (3^6) packing occurs at high packing fraction for the regular octagon. At higher N ($N > 9$), the assembly is of disk type. The regular decagon is a disk class assembly and forms a rhombic crystal structure at lower packing fraction (see Figure 4.3i). Furthermore, the hendecagons, and tridecagon both self-assemble a sheared $(3^2.4.3.4)$ Archimedean tiling (see Figure 4.3f, 4.3k). The final transformation between the sheared $(3^2.4.3.4)$ Archimedean tiling and the (3^6) Archimedean tiling consumes the remaining part of the n -gon family. The disk class assemblies occur at high N highlighting the transition between faceted and continuous building blocks.

4.5.2 Pinching

The pinching transformation alters the geometry of the polygonal nanoplates by moving a vertex radially from the center (see Figure 4.4b). We investigate the pinching transformation while maintaining a convex building block. The pinching transformation provides a geometric transformation between a polygon with (n) vertices and an extended vertex to a polygon with $(n-1)$ vertices and one large edge, analogous to the transformation between a sphere and a cone. Previous work on conic self-assembly has shown that a precise sequence of convex clusters form at magic numbers. *Chen et al. (2007a)* To quantify the transformation, we introduce a deformation parameter, ξ ; this parameter provides a means of geometrically connecting these two building blocks, which can have dramatically different phase behavior. Figure 4.4a shows the phase behavior of each building block in a geometric phase diagram between faceting and pinching. The regular n -gons at $\xi=0.5$ are shown with the symbols and crystal structures observed in Fig 4.3. If the assembly of the pinched building block is crystallographically indistinguishable from the regular n -gon (such as the regular tri-

angle, undecagon, dodecagon, and hendecagon), the regular polygon symbol is used to denote the crystalline structure. (See Figure 4.4a) We report that at low N, the pinch transformation can have a dramatic effect on assembly, and at higher N, assembly is not affected. As N increases, the convexity constrains the extent of the pinch transformation so that at high N the deformation can only be small.

The pinch transformation of the square stabilizes two kite assemblies shown in Figure 4.4c-d. A kite is a specific quadrilateral with two pairs of adjacent equal-length sides; kites are a prototile of the famous Penrose quasicrystalline tiling. The pinch transformation stabilizes two alternating crystal structures. The first crystal structure is a hierarchical tiling found at $\xi=0.0$ and $N=4$ (See Figure 4.4c). The unit cell consists of two kites that combine to form a rhombus. The rhombus tiling is similar to the (4^4) Archimedean tiling except for a shift between each row of rhombuses due to the small protrusion of the pinched vertex. (See Figure 4.4b-c) Hierarchical crystals assembled with nanoparticles has been shown to have interesting mechanical *Miszta et al.* (2011) and electronic *Tao et al.* (2012) properties. The second crystal structure is composed of an alternating pattern of kites, which is topologically equivalent to the (4^4) Archimedean tiling. Pinching can affect the assembly greatly, as shown in the hierarchical assembly, or distort the basic tiling of the shape.

The pinch transformation of the pentagon leads to two distinct crystal structures; the crystal structures observed are the pentagonal Cairo tiling at $\xi=0.25$ and $N=5$ (Figure 4.4e), and a hierarchical rectangular tiling at $\xi=0.0$ and $N=5$ (Figure 4.4f). The pentagonal Cairo tiling is the dual of the $(3^2.4.3.4)$ Archimedean tiling, and is also referred to as the $((5^3)^2.5^4.5^3.5^4)$ McMahan net. *O’Keeffe and Hyde* (1980) The Fe atoms in $Bi_2Fe_4O_9$ have a pentagonal Cairo tiling, and this material has neighboring antiferromagnetic interactions *Ressouche et al.* (2009) in a noncollinear magnetic structure. At the nanoscale, three- and four-arm DNA junction tiles have been shown to self-assemble the pentagonal Cairo tiling. *Zhang et al.* (2013) At lower

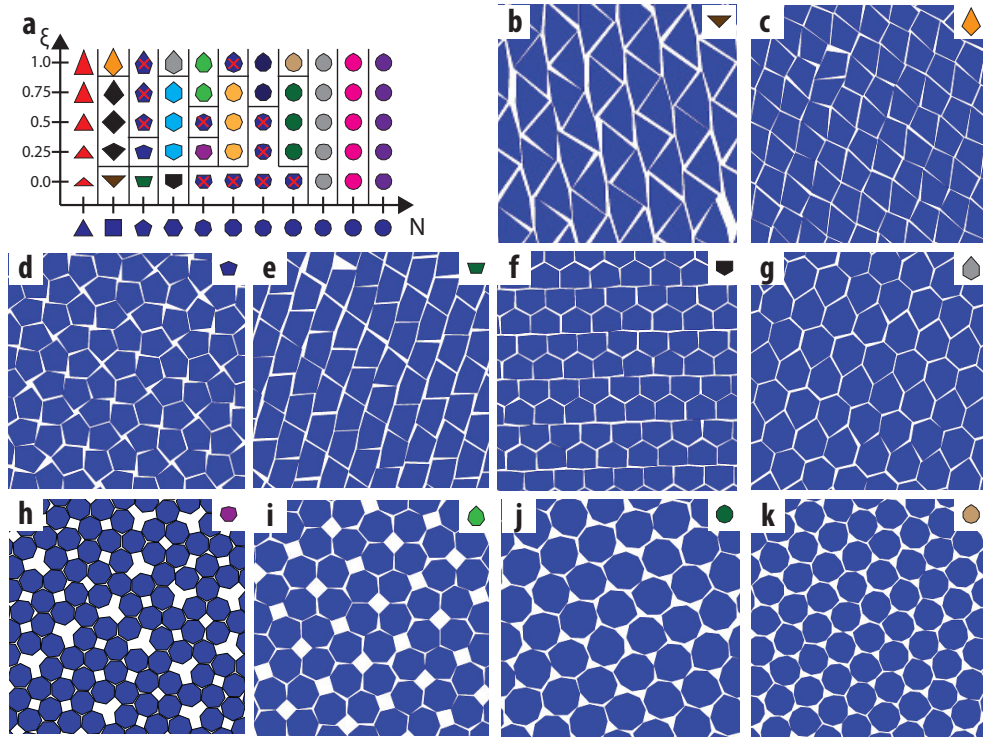


Figure 4.4: The effect of the pinch transformation on the assembly of polygonal nanoplates is summarized above. A geometric phase diagram of faceting and pinching anisotropy dimensions is shown above (a). The building blocks for each geometric phase point are shown in the geometric phase diagram (a). Representative snapshots of all crystal structures observed by applying the pinch transformation are shown for the regular polygons between the regular triangle, and the regular hendecagon. The regular n -gons at $\xi=0.5$ are shown with the symbols and crystal structures observed in Fig 4.3. The assemblies for the pinched n -gon family are a shortened kite assembly with pmg symmetry for $\xi=0.0$ and $N=4$ (b), a lengthened kite assembly with pmg symmetry for $\xi=0.0$ and $N=4$ (c), the pentagonal Cairo tiling for $\xi=0.25$ and $N=4$ (d), a trapezoidal assembly with for $\xi=0.0$ and $N=5$ (e), a shifted prismatic pentagon tiling for $\xi=0.0$ and $N=6$ (f), a lengthened hexagon with alternating rows in a triangular tiling for $\xi=1.0$ and $N=6$ (g), a shortened heptagon dodecagonal quasicrystal for $\xi=0.25$ and $N=7$ (h), a lengthened heptagon ($3^2.4.3.4$) Archimedean tiling for $\xi=0.75$ and $N=7$ (i), a lengthened nonagon triangular tiling for $\xi=0.75$ and $N=9$ (j), a lengthened decagon triangular tiling for $\xi=0.75$ and $N=10$ (m).

ξ , the hierarchical rectangular crystal structure forms. Its unit cell consists of two pinched pentagons that collectively form a rectangle; the rectangular crystal structure is similar to the (4^4) Archimedean tiling except that the tiling is stretched along the apothem of the building block.

The pinch transformation for the hexagon stabilizes two different crystalline structures. (See Figure 4.4g,h) The crystal structures observed are a hierarchical tiling closely related to the prismatic pentagonal tiling at $\xi=0.0$ and $N=6$, and an alternating hexagonal tiling $\xi=0.0$ and $N=6$. (See Figure 4.4g,h) The prismatic pentagonal tiling is the dual of the $(3^3.4^2)$ Archimedean tiling. Three- and four-arm DNA junction tiles have also been shown to self-assemble the prismatic pentagonal tiling. *Zhang et al.* (2013) At high pinching ($\xi > 0.75$), the pinched hexagon forms an alternating crystal structure similar to the (6^3) Archimedean tiling. The pinched hexagon can self-assemble an alternating crystal structure and the prismatic pentagonal tiling.

The pinch transformation of the heptagon stabilizes the snub square (SS) Archimedean tiling and the dodecagonal shield quasicrystal. *Stampfli* (1986) At both low and high ξ , the SS Archimedean tiling is stable (Figure 4.4i). At low ξ , the shield dodecagonal quasicrystal is stable (Figure 4.4k). A disordered region exists around the regular heptagon at intermediate ξ . Under each crystalline structure, we show the heptagonal nanoplates that self-assemble the crystalline structure. It is interesting to note that the SS tiling, also known as the σ -phase *Frank and Kasper* (1958), is in close proximity geometrically to the dodecagonal quasicrystal. Simple modifications of crystalline growth rules have been shown to control the stability region of the σ -phase and the dodecagonal triangle square tiling. *Kuo et al.* (1988) Patchy particles with seven patches arranged in a heptagonal arrangement also form a dodecagonal quasicrystal. *van der Linden et al.* (2012) It is notable that the quasicrystal is stable for an irregular arrangement of facets on the polygonal nanoplates. (See Figure 5) The pinch transformation provides a means of transforming the disordered heptagon

assembly into the snub square and a dodecagonal quasicrystal and provides design rules for tuning between these two structures.

At high N , the pinching deformation is constrained to small changes by the convexity and vertex constraints. (See Figure 4.4a,b) The pinched octagon at high pinching forms only disordered assemblies. (See Figure 4.4a) The nonagon and decagon at high ξ form a triangular crystal structure. For the pinched nonagon and decagon, the packing and assembly becomes the same crystal structure. When the packing and self-assembly are the same, the assembly is expected to have high yield. (See Chapter 3) For the undecagon, dodecagon, and hendecagon, the pinching transformation has no effect on assembly.

4.5.3 Elongation

The elongation transformation alters the geometry of the polygonal nanoplates by elongating two symmetric edges of a nanoplate. Notice that this transformation can only be applied on polygons with an even number of edges. At large elongation, the transformation transforms nanoplates into faceted nanorods. *Nikoobakht and El-Sayed* (2003) The elongation transformation is equivalent to the transformation between a sphere and the spherocylinder. The transformation is also closely related to the elongation along an axis of a sphere to form an ellipsoid. Patchy and hard spherocylinders *Veerman and Frenkel* (1990); *Vácha and Frenkel* (2013) and ellipsoids *Frenkel* (1984); *Liu et al.* (2012a) are the natural systems which to compare the phase behavior of elongated faceted nanoplates. The deformation parameter ξ quantifies the degree of elongation. We show the phase behavior of each building block in a geometric phase diagram between faceting and elongation. (See Figure 4.5a) The regular n -gons at $\xi=0.5$ are shown with the symbols and crystal structures observed in Fig 4.3. (See Figure 4.5a) The elongated building blocks used to create the assemblies are displayed next to the phase diagram panel. (See Figure 4.5b) The elongation

transformation effects the assembly of n-gons from squares to dodecagons.

The elongated square self-assembles a rectangular tiling closely related to the (4^4) Archimedean tiling. (See Figure 4.5c) The rectangular assembly is rotationally degenerate, yet remains on the (4^4) Archimedean lattice points. Molecular rectangles *Li et al.* (2007) at higher elongation form a stretched (4^4) Archimedean crystal structure. The elongated square forms a crystal structure closely related to the square.

The elongated hexagon self-assembles into three distinct crystal structures: a porous rhombille tiling (Figure 4.4e), an aperiodic rhombus tiling (Figure 4.4d), and an elongated (6^3) Archimedean tiling. (Figure 4.4f) At low elongation ($\xi=0.25$ and $N=6$), the elongated hexagon forms the rhombille tiling. (See Figure 4.4d), which is the dual of the $(3.6.3.6)$ Archimedean tiling. Rhombille tilings are observed in layered perovskites. *Wang and Ran* (2011) Density functional theory calculations (DFT) of off-lattice rhombus tiles showed the stability of the rhombille tiling for asymmetric patches. *Wang and Ran* (2011) Here, we report that this is the first assembled porous rhombille tiling. At lower elongation ($\xi=0.0$ and $N=6$), the elongated hexagon forms a random tiling of rhombuses (See Figure 4.4e) This result is in agreement with the DFT calculations of molecular rhombs. *Whitelam et al.* (2012) At high elongation ($\xi=1$), the elongated hexagon forms a stretched (6^3) Archimedean tiling; EuF_3 elongated hexagonal nanoplates *Ye et al.* (2013c) form this crystal structure.

At low elongation ($\xi=0.0$), the elongated octagon forms a triangular tiling (See Figure 4.5h), whereas at high elongation, the elongated octagons forms a stretched (4.8^2) Archimedean tiling. (See Figure 4.5g)

The elongated decagon forms an alternating and a stretched rhombic crystal structure. (See Figure 4.5i,j) The alternating crystal structure consists of alternating rows of oriented elongated decagons at $\xi=0$. The unit cell of this crystal structure consists of two decagons with different orientation and tiles space in a rectangular lattice. (See Figure 4.5i) To our knowledge, the alternating elongated decagon crystal structure

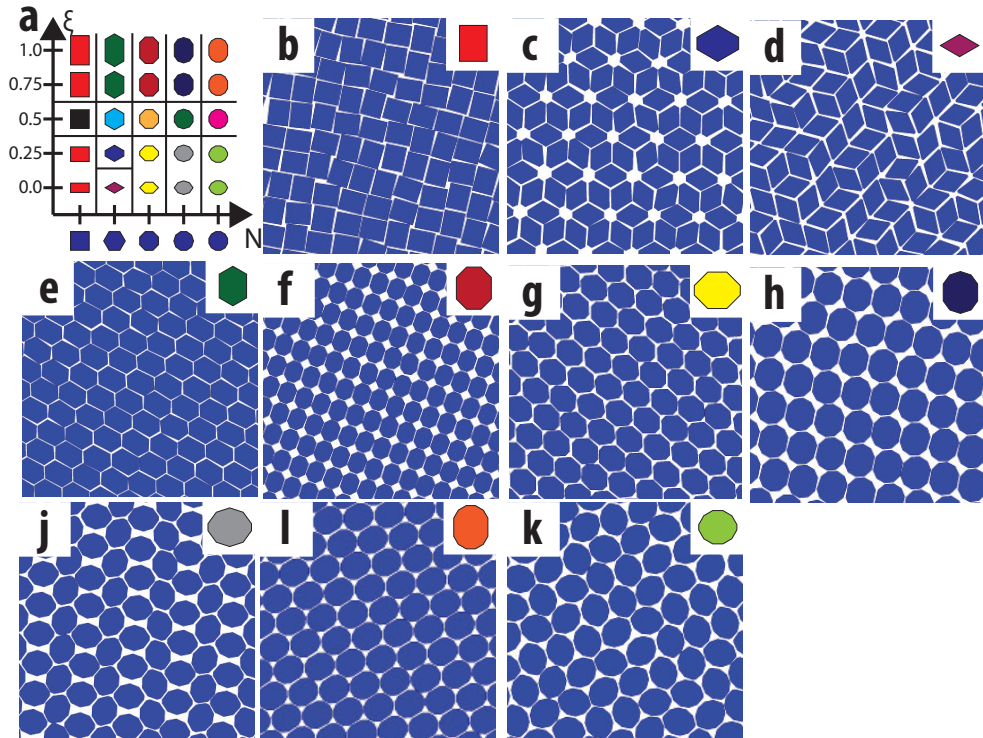


Figure 4.5: The effect of the elongation transformation on the assembly of polygonal nanoplates is summarized above. A geometric diagram between the faceting and elongation anisotropy dimensions shows the crystalline phases observed (a). The building blocks for each geometric state point are shown in the geometric phase diagram (a). Representative snapshots for all crystal structures observed for elongated polygons are shown above. The regular n -gons at $\xi=0.5$ are shown with the symbols and crystal structures observed in Fig 4.3. The assemblies for the elongated n -gons are an elongated rectangle crystal structure at $\xi=0.25$ and $N=4$ (b), a shortened hexagon with a porous rhombile crystal structure at $\xi=0.25$ and $N=6$ (c), a shortened hexagon with an aperiodic rhombus tiling at $\xi=0.0$ and $N=6$ (d), an elongated hexagon with stretched (6^3) Archimedean tiling at $\xi=0.75$ and $N=8$ (e), an elongated octagon with stretched (4.8^2) Archimedean tiling at $\xi=0.75$ and $N=8$ (f), a shortened octagonal triangular crystal structure at $\xi=0.75$ and $N=8$ (g), an elongated decagonal triangular crystal structure at $\xi=0.75$ and $N=10$ (h), a shortened decagon with a porous alternating triangular crystal structure at $\xi=0.75$ and $N=10$ (i), an elongated dodecagon with a stretched (3.12^2) Archimedean tiling at $\xi=0.75$ and $N=12$ (j), a shortened dodecagon with a rotationally degenerate triangular lattice at $\xi=0.25$ and $N=12$ (k).

has, to our knowledge, not been observed experimentally. At high elongation ($\xi=1$), a stretched rhombic crystal structure forms. (See Figure 4.5j)

The elongated dodecagon forms a stretched Archimedean tiling and a triangular tiling. (See Figure 4.5l,k) The elongated dodecagon forms a stretched (3.12^2) Archimedean tiling at $\xi=1$. In a similar way to the elongated hexagon, octagon, and decagon, the elongated dodecagon stretches the regular polygons crystal structure. At lower elongation at $\xi=0$, the dodecagon forms a triangular lattice that is rotationally degenerate. (See Figure 4.5k)

Clearly, the elongation transformation is not symmetric in that low and high elongation n-gons do not self-assemble the same crystal structure. It is interesting to note that the phase diagram of hard ellipsoids is symmetric *Frenkel* (1984), which implies that faceting can have an important effect on the assembly of nanorods at low aspect ratio *Sau and Murphy* (2004). For nanoplates, the elongation transformation has been previously studied for lanthanide fluoride (LaF_3) nanoplates both experimentally and with simulations. *Ye et al.* (2013c) These simulations results revealed that for systems with symmetric interactions, parallel arrangements were stable regardless of the degree of elongations; entropic interactions favored such arrangements, and the introduction of symmetric forces (comparable to thermal energies) were not expected to disrupt the trend. *Ye et al.* (2013c) In fact, simulations *Ye et al.* (2013c) reveal that elongation leads to the formation of tetragonal lattices since these arrangements maximize the amount of contact between neighboring particles, thus the global contribution to the free energy by the enthalpic and entropic interactions is minimized. *Ye et al.* (2013c)

4.5.4 Truncation

The truncation transformation of faceted nanoparticles alters the geometry of the polygonal nanoplates by truncating each vertex symmetrically into an edge. The

symmetric truncation transformation has no analogue in continuous geometries (disks and ellipses), and is characteristic of faceted nanoparticles. Truncation transforms an initial polygon with n vertices into another polygon with twice the number of vertices. (See Figure 4.6b) We introduce a deformation parameter ξ to quantify this transformation. . We show the phase behavior of each building block in a geometric phase diagram between faceting and truncation. (See Figure 4.6a) The regular n -gons at $\xi=0.0$ and their crystal structures are shown as in Fig 4.3. (See Figure 4.6a) The truncation transformation ends in a regular polygon, so at $\xi=1.0$ the regular n -gons phase behavior is observed. (See Figure 4.6a) The truncated building blocks used to create the assemblies are placed next to the phase diagram panel. (See Figure 4.6b) Truncation has an effect on self-assembly at low N , but at higher N the particles emulated the phase behavior of a disk. *Chen et al.* (2002)

The truncation transformation transforms the triangular nanoplate into a hexagonal nanoplate. The triangular and hexagonal nanoplates form Archimedean tilings. (See Figure 4.7) In 3D, the truncation of tetrahedra transformed the assemblies from a quasicrystal to a bcc crystal structure. *Damasceno et al.* (2012a) However, in 2D, truncation does not have a profound effect. The truncated triangle forms the (3^6) Archimedean tiling. Halfway between the triangular and hexagonal nanoplates the assembly flips from the (3^6) Archimedean tiling to the (6^3) Archimedean tiling. The intermediate crystal structure is a porous triangular crystal structure. (See Figure 4.6c) The continuous transformation between the (3^6) Archimedean tiling to the (6^3) Archimedean tiling shows that geometric transformation can have subtle, gradual effects on the self-assembly properties.

The truncated octagon and square form crystalline structures that are closely related. The truncated square at intermediate truncation $\xi = 0.25$ forms a Mediterranean tiling. (See Figure 4.6d) The Mediterranean tiling is similar to the (4.8^2) Archimedean but the square tile is either smaller or truncated. (See Figure 4.6d) The

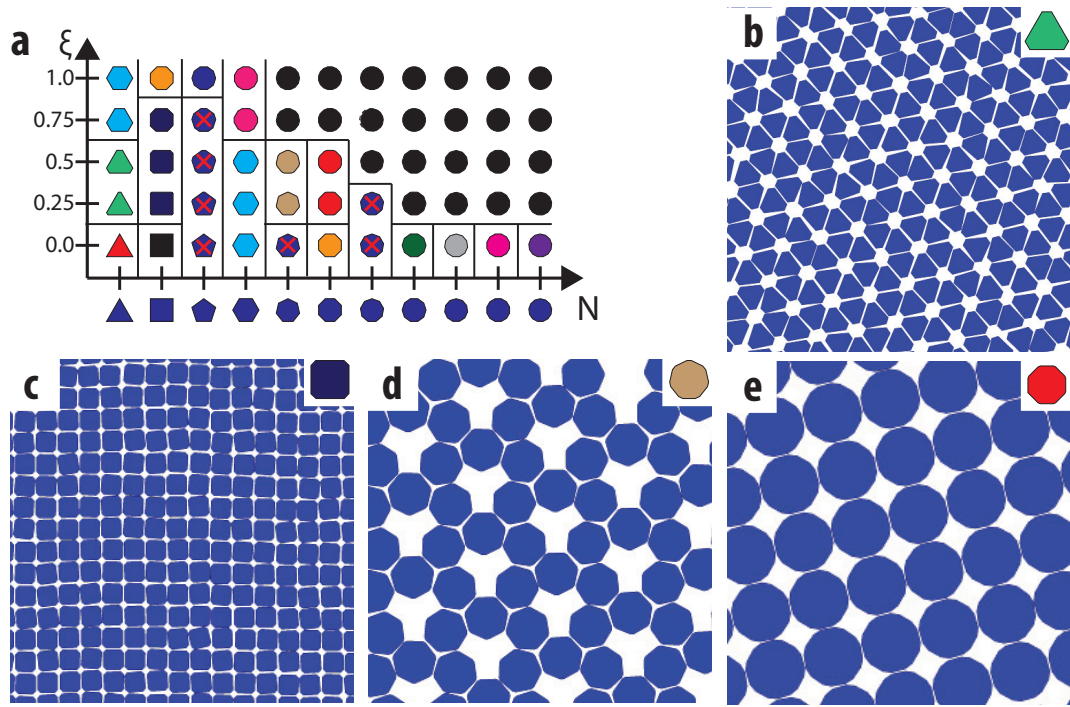


Figure 4.6: The effect of the truncation transformation on the assembly of polygonal nanoplates is summarized above. A geometric diagram between the faceting and truncation anisotropy dimensions shows the crystalline phases observed (a). The building blocks for each geometric state point are shown on the geometric phase diagram (a). Representative snapshots for all crystal structures observed for truncated polygons are shown above. The regular n -gons at $\xi=0.0$ are shown with the symbols and crystal structures observed in Fig 4.3. The assemblies for the truncated n -gons are a truncated triangle with a porous (3^6) Archimedean tiling at $\xi=0.25$ and $N=3$ (b), a truncated square forms a Mediterranean tiling at $\xi=0.5$ and $N=4$ (c), a truncated heptagon forms a hexagonal shield tiling at $\xi=0.5$ and $N=7$ (d), and a truncated octagon form a regular star polygon tiling at $\xi=0.5$ and $N=8$ (e).

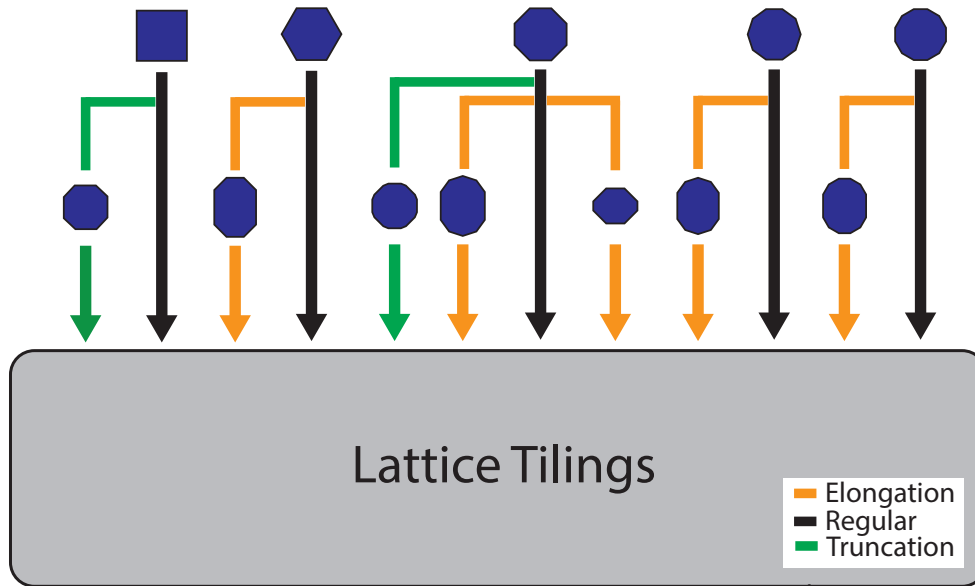


Figure 4.7: A summary of all the transformed nanoplates that form lattice tilings. Elongated hexagons, octagons, decagons, and dodecagons form lattice tilings. Regular squares, hexagons, octagons, decagons, and dodecagons form lattice tilings. Also, truncated squares and octagons form lattice tilings.

truncated octagon forms an irregular star polygon tiling. *Grünbaum and Shephard* (1977) This irregular star polygon tiling is closely related to the $((8.4_{\pi/4}^*)^2.8.4_{\pi/4}^{**})$ regular star polygon tiling formed by symmetric truncation. *Grünbaum and Shephard* (1977) Similarly, closed packed assemblies of PbS nanostars have been achieved by vertical deposition. *Huang et al.* (2010) The truncated octagon provides a simple means of obtaining patterned array of porous stars. The truncation of regular n-gons with a large number of vertices alters the pore structure, but not the coordination of the crystal structure.

The truncated heptagon stabilizes a triangular shield tiling. (See Figure 4.6e) The triangular shield tiling is one of the 63 convex isogonal tilings. *Grünbaum and Shephard* (1978) Isogonal tilings are tilings whose symmetry group acts on the vertices. The truncated heptagon crystal structure is porous and forms at low truncation $\xi=0.5$. At higher truncation at $\xi=0.75$, the truncated heptagon acts like a disk. The proximity of these state points motivates the possibility of a switchable structure.

4.6 Discussion

The shape optimization of faceted nanoparticles for assembly begins with understanding the effect of different geometric transformations on the assembly of polygonal nanoplates. Each geometric transformation provides the material designer with a new design axis to synthesize the functional materials of the future. Truncation and elongation allow the synthesis of porous tilings such as the porous rhombile tiling and the porous shield triangle isogonal tilings. (See Figure 4.6e,4.5d) Pinching allows for the stabilization of the pentagonal Cairo tiling or the prismatic pentagonal tiling. (See Figure 4.4e, g) The poor assemblers in the regular n-gon class, such as the nonagon, heptagon, and pentagon, can be self-assembled into crystal structures by judicious use of one of the geometric transformation established in the nanoplates literature.

Our results can be divided into three classes of crystals: lattice, porous, and complex tilings. (See Figure 4.7,4.8,4.9) A few crystal structures also exhibit random and rotationally degenerate tilings. Lattice tilings, or isohedral tilings *Grünbaum and Shephard* (2008), are tilings that can be constructed by a single translation vector. (See Figure 4.7) It is notable that only the truncation and elongation transforms lead to lattice tilings and that only nanoplates with even numbers of vertices have lattice tilings. It is clear that these lattice tilings arise in highly symmetric particles. The second class of crystals is porous tilings. (See Figure 4.7) We report the first recorded porous tilings made from faceted particles. We find that only asymmetric hexagons and heptagons form porous tilings. (See Figure 4.8) Experimental work on metal organic frameworks has shown highly stable porous crystalline structures. *Li et al.* (1999) The benefit of using irregular faceted polygonal nanoplates is that the pore size can be dynamically tuned via truncation using photodecomposition. The third class of crystalline structures is complex crystals with multiple building blocks in a unit cell. (See Figure 4.9) This class of crystals is observed for irregular square pentagons hexagons and decagons. The majority of the complex crystals occur due

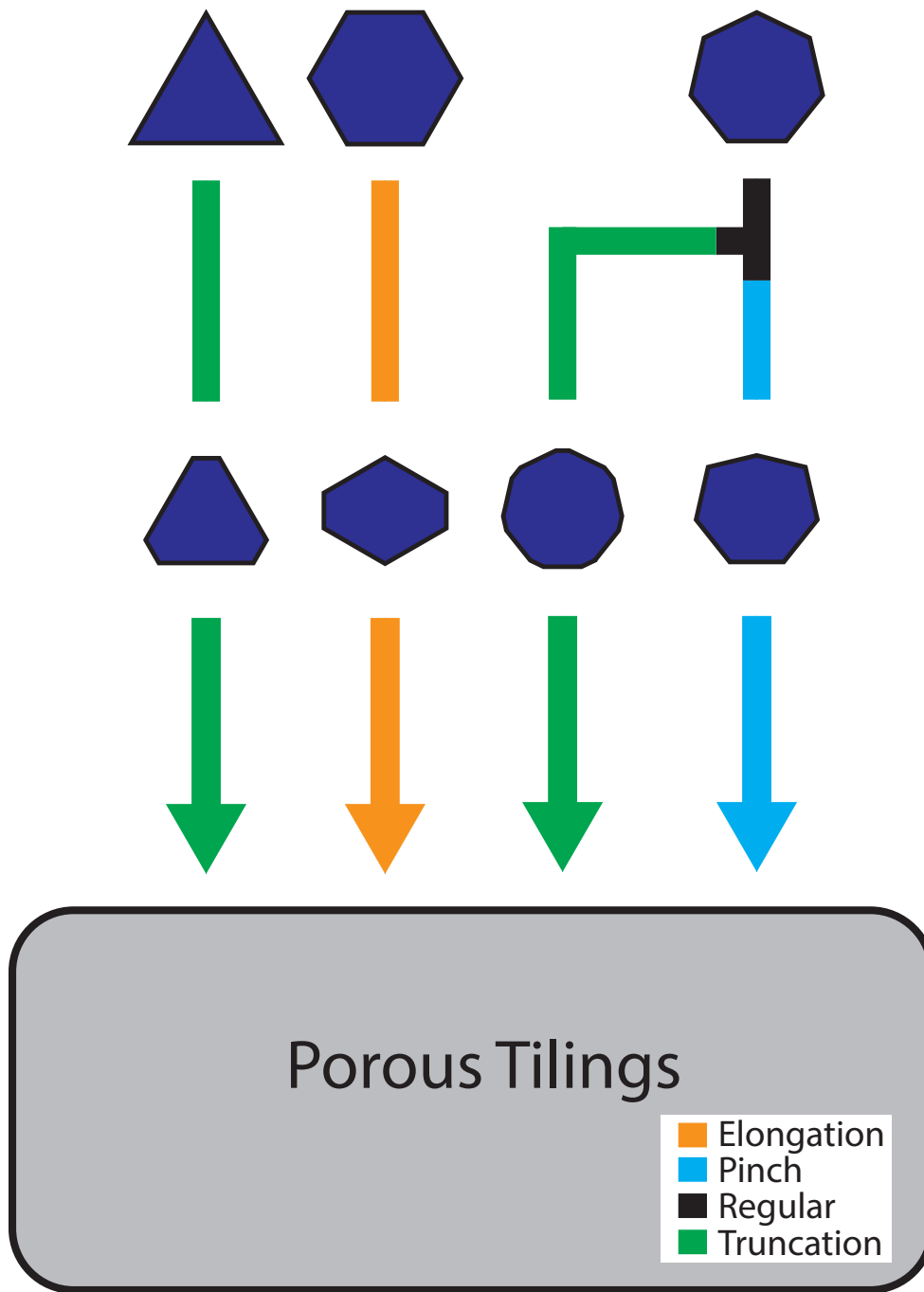


Figure 4.8: A summary of all the transformed nanoplates that form porous tilings. Elongated hexagons, pinched and truncated heptagons, and truncated triangles form porous tilings.

to the pinch transformation and at low N . (See Figure 4.9) The complex crystalline class contains interesting tilings such as the pentagonal Cairo tiling. (See Figure 4.4) The location of these interesting structures on the extended geometric phase diagram (pinched low N polygonal nanoplates) highlights the need for experimental studies on monodisperse irregular nanoplates. The rotational degenerate tilings are found in pinched nonagons and decagons and elongated dodecagons. The orientationally degenerate dodecagon crystal structure is expected since elongated pear-like colloidal dimers also form disordered rotator crystal structures. *Hosein et al.* (2009) On the other hand, the orientationally degenerate crystal structure of asymmetric pinched nonagons and decagons is analogous to the assembly of hard asymmetric dimers. *Milinković et al.* (2013)

From the perspective of material optimization, the improved assembly properties of the regular heptagon highlight the power of shape transformations. The frustrated assembly of the regular heptagon has two local motifs at low densities. These local motifs are the snub square ($3^2.4.3.4$) Archimedean tiling and the shield-triangle tiling. Both motifs are observed in the shield dodecagonal quasicrystal. The pinch transformation allows for the self-assembly of the snub square and the dodecagonal shield quasicrystal structures. The truncation transformation allows for the self-assembly of the shield-triangle tiling. These geometric transformations provide a geometric means of toggling between different assembly types. The judicious use of geometric transformations could lead to the self-assembly of crystal structures of increasing complexity.

4.7 Conclusion

Building an experimental toolbox for self-assembly that rivals the established engineering methods of circuit design or power plant design could transform the field of self-assembly from a basic scientific discipline to an engineering discipline. The development of heuristic rules for the optimization of shape allows the practicing experi-

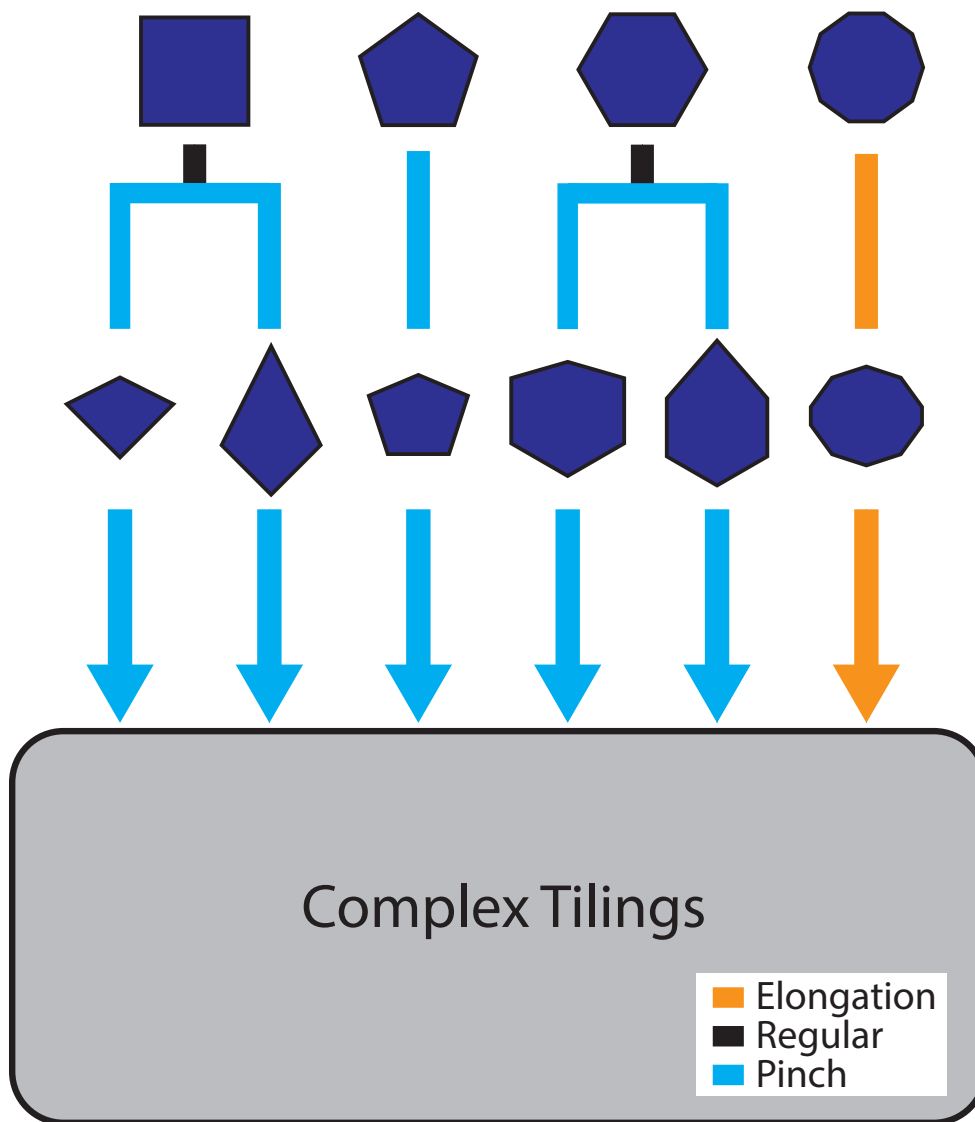


Figure 4.9: A summary of all the complex nanoplates that form lattice tilings. Pinched square, pentagon, hexagons form complex tilings. Pinched square and hexagons form complex tilings at high and low pinching. The elongated decagon forms a complex tiling.

mentalist to tune the anisotropic building block to improve the crystalline properties of the proposed nanomaterials. Furthermore, an understanding of the mechanisms to improve the crystallinity of self-assembly materials could allow for a priori screening of materials. We look forward to experimental developments to validate the material design principles provided in this article

CHAPTER V

Outlook

The use of anisotropy dimensions to improve the self-assembly properties of nanomaterials is in its infancy. Although theoretical frameworks on the effect of shape on assembly exist *van Anders et al.* (2013c,b), these framework only explain the phenomenological forces present in faceted nanoparticles. To begin engineering nanoparticle assemblies in the way VLSI components are designed, a great deal of work needs to be done correlating self-assembly with building block attributes. A tool that would guide systematic design of building blocks for self-assembly is sorely needed. Such a tool could greatly speed up material design. Even though a great deal of work needs to be done, actionable conclusions can be extracted from the self-assembly experiments performed above. The conclusions can be divided into three groups: multifunctional materials, dynamic materials, and machine learning.

5.1 Multifunctional Materials

Multifunctional materials are materials with enhanced properties that are endowed with functional groups that control their interactions. The interest in multifunctional materials arises from the desire to enhance material properties and to combine different properties into one material. Multifunctional materials have been used in organic electronic *Forrest* (2004), sensors *Medintz et al.* (2005), and memory *Möller et al.*

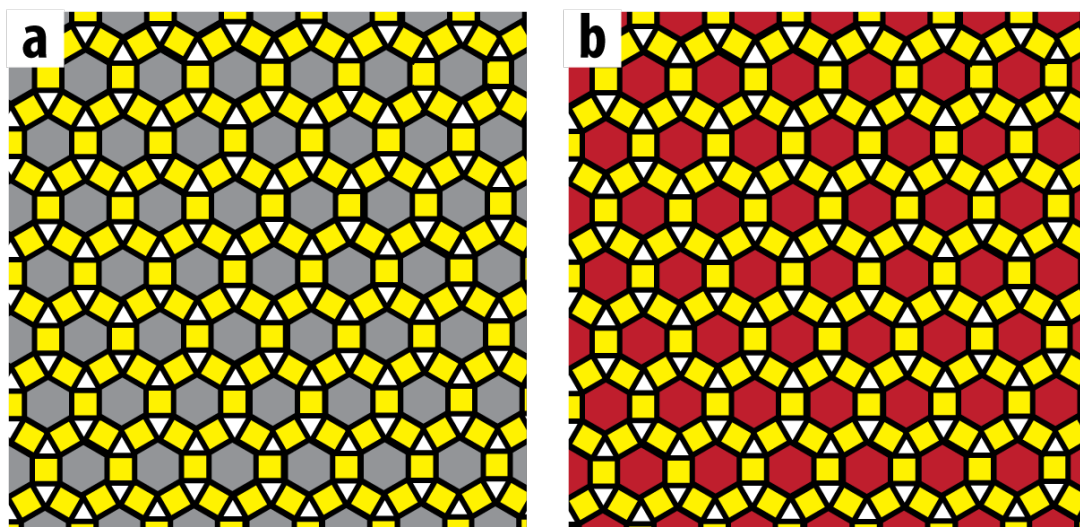


Figure 5.1: The power of ligand driven self-assembly is the ability to substitute different materials into crystal structures. We highlight how materials can be substituted in the rhombitrihexagonal tiling (3.4.6.4) Archimedean tiling. The two material combinations are gold square nanoplates combined with silver hexagonal nanoplates(a), and gold square nanoplates combined with CdSe hexagonal nanoplates.

(2003) applications. The interaction designs observed for the Archimedean tilings highlight the importance of controlling the specificity of ligands. If the ligand-ligand van der Waals interactions drive assembly, the constituent materials of the nanoplates plays a secondary role in self-assembly and the designs observed in Chapter 3 take on a greater meaning. The interactions designs allow for material substitution. If the effective interaction strength and size ratio between nanoplates is conserved, CdSe can be substituted for silver nanoplates to form the rhombitrihexagonal(3.4.6.4) Archimedean tiling. Materials substitution allows for the substitution of semiconductor nanoplates by noble metal nanoplates or the substitution of metal nanoplates by polymer nanoplates, which could fundamentally alter how one synthesizes, ponders, and designs multifunctional nanomaterials.

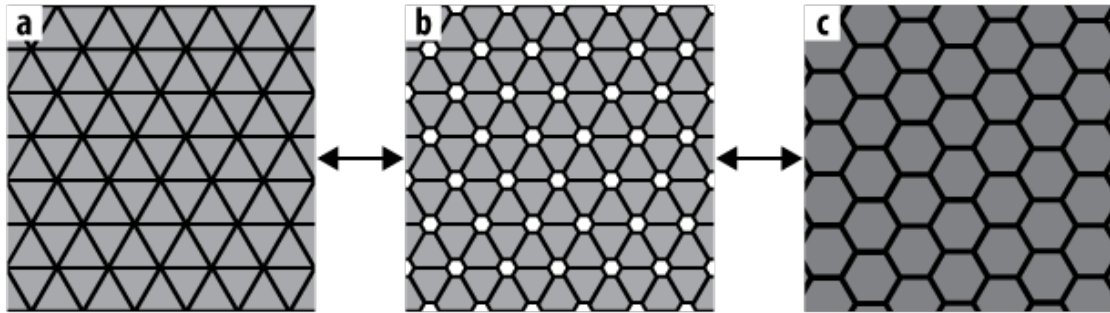


Figure 5.2: An example transformation of a dynamic materials using geometric transformations. Silver nanoplates can transform from triangular(a) to hexagonal(c) through symmetric truncation. An intermediate porous crystal structure made from truncated hexagons is observed in this transformation.(b)

5.2 Dynamic Materials

Dynamic materials are materials whose properties change over time. The properties change due to a response towards external stimuli. Self-healing materials are capable to partially or completely heal damage inflicted to the material. Cross-linked chemical gels can heal autonomously through the addition of arylbenzofuranone cross-linker. *Imato et al.* (2012) Self-assembled hydrogen-bonded thermoplastic elastomers combine toughness with self-healing. *Chen et al.* (2012b) External stimuli can toggle molecular switches enhanced with nanoparticles between different material states. *Kay et al.* (2007); *Klajn et al.* (2009a) Functionalized nanoparticles controlled by the redox potential can acts as a controllable reversible sponge for targeted release of drugs. *Klajn et al.* (2009b) UV irradiation *Zhang et al.* (2009) and thermal processes *Sun et al.* (2003) can transform triangular silver nanoplates into different shapes. The ability to alter the shape of the nanoparticle *insitu* is potentially a new paradigm for dynamic materials. Shape change in nanoparticles is to known to improve the kinetics of self-assembly. *Nguyen et al.* (2011) However, one of the great challenges of dynamic materials via shape change is how to design the shape transformation.

The transformations in Chapter 4 provide guidelines for these dynamic materials. An example transformation for a dynamic material is shown in Figure 5.2. The transformation alters the building block between a triangle, truncated triangle, and hexagon. (See Figure 5.2a, 5.2b, 5.2c) The geometric transformation provides a mechanism of tuning the porosity, which can be applied to nanoswitches *Vlassiouk et al.* (2006); *Xia et al.* (2008) via self-assembly.

5.3 Machine Learning

Machine learning is a part of theoretical computer science which creates systems that learn from data. Machine learning has been used to resolve problems ranging from oil spill detection *Kubat et al.* (1998) to fraud detection *Fawcett and Provost* (1997). The representation of the data is a key step in any machine learning process. The representation of the data is built upon the human intuition towards the problem. *Goldberg and Holland* (1988) The questions answered in this thesis provide the basis for this intuition. The project on the Archimedean tilings provides intuition on how to design and alter the chemical specificity of the polymer coatings of nanomaterials. The project on geometric transformations provides insight on the effect of different transformations on self-assembly. The pacman project highlights how the selection of the correct anisotropy dimensions is critical to the self-assembly of certain crystal structures. In a word, each project highlights how to define the training data for a machine learning algorithm. *Batista et al.* (2004) In Figure 5.3, a sketch of a machine learning algorithm is explored. The machine learning algorithm is divided into two parts: the training and learning part. The training part consists of an exploratory part on experimentally relevant anisotropic dimensions. (See Figure 5.3) A collection of state points exploring each anisotropy dimensions is defined. A self-assembly experiment is performed for each one of these state points. (See Figure 5) A clustering algorithm *Fisher* (1987), a form of unsupervised machine learning,

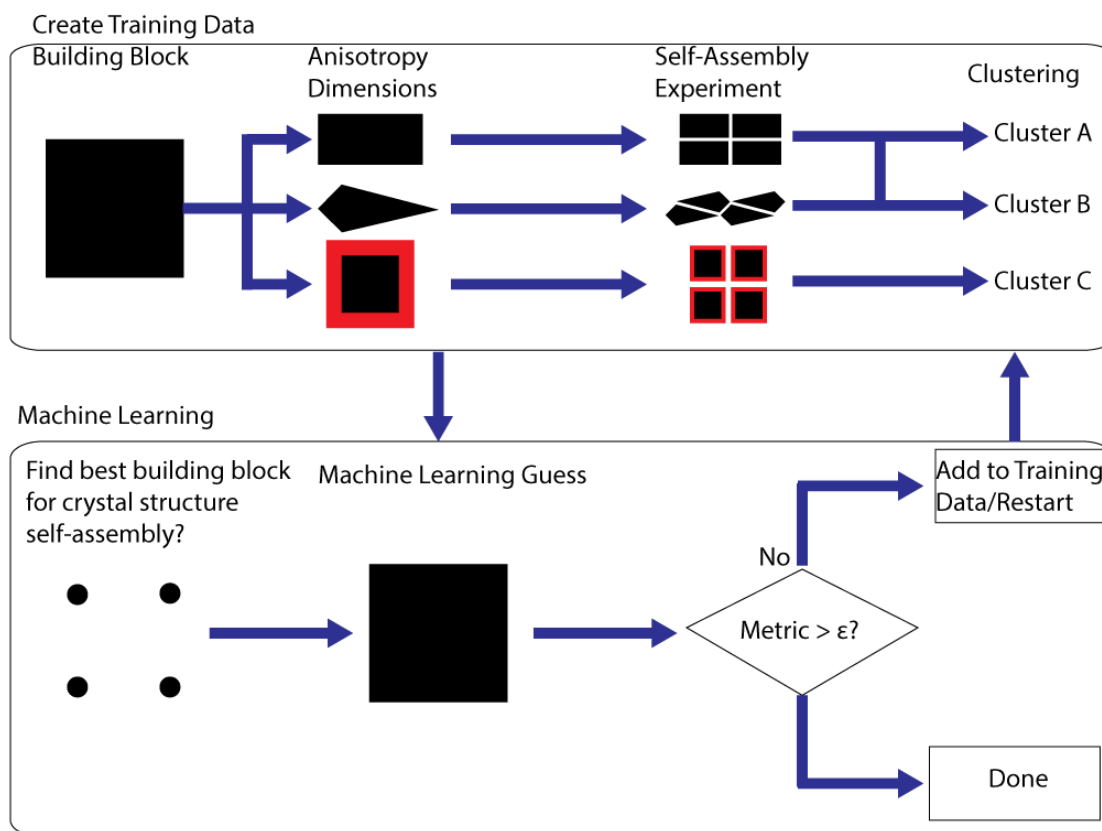


Figure 5.3: A sketch of a machine learning algorithm. The algorithm is divided into a training and learning part. The training part explores the anisotropy dimensions and categorizes the data using a machine learning algorithm. After training, questions can be asked of the data.

is used to group the salient structural features of the self-assembly experiment. An example grouping could be the crystallographic point group, but a successful machine learning algorithm would use a collection of different metrics. (See Figure 5.3) With the training data, queries can be performed to guess the self-assembly properties of different building blocks. Should the machine learning algorithm succeed, the answer is returned to the user. Upon failure, information is added to the training data to improve the self-assembly selection process.

APPENDICES

APPENDIX A

Simulation Parameters for Lock-Key Colloids

The supplementary information is divided into three sections. The first section describes the simulation parameters and tabulates information on quasi-3D state points.

Colloidal Molecules Simulation Parameters

Parameters	Lock	Key	Lock-Key
σ	0.5	0.5	0.5
α	6.0	6.0	6.0
δ	0.33σ	0.0σ	0.165σ
ϵ	$1.0k_B T$	$1.1k_B T$	$1.75k_B T$
ζ	250	520	380

Simulation parameters used for our potential are summarized above. (See Table S1)

The definition of these parameters are covered in the main text.

Crystal structures observed in Quasi-3D Simulations

N_L	D_L	Lock-Key	Crystal Structure
1	1.3	0.5	Dis
1	1.3	0.3	Dis
1	1.5	0.3	Dis
1	1.5	0.4	PbO
1	1.5	0.5	PbO
1	1.7	0.5	PbO
2	1.3	0.4	$L_{HH}^2 K_D$
2	1.3	0.5	$L_{HH}^2 K_D$
2	1.5	0.3	Dis
2	1.5	0.4	Dis
2	1.5	0.3	$L_{HH}^2 K_D$
2	1.7	0.3	Dis
2	1.7	0.4	Dis
2	1.7	0.5	$L_{HH}^2 K_D$
3	1.3	0.1	Dis
3	1.3	0.2	Dis
3	1.3	0.3	Dis
3	1.5	0.1	Dis
3	1.5	0.2	Dis
3	1.5	0.3	Dis
3	1.7	0.1	Dis
3	1.7	0.2	Dis
3	1.7	0.3	Dis
4	1.2	0.4	$L_H^4 K_D$

4	1.3	0.0	Dis
4	1.3	0.1	Dis
4	1.3	0.2	Dis
4	1.3	0.3	$L_H^4 K_D$
4	1.3	0.4	$L_H^4 K_S$
4	1.5	0.0	Dis
4	1.5	0.1	Dis
4	1.5	0.2	Dis
4	1.7	0.0	Dis
4	1.7	0.1	Dis
4	1.7	0.2	Dis

Geometric parameters for the Quasi-2D simulation are summarized above. (See Table S2) Simulations were performed for a range of lock number ($N_L=1-4$), overlap ($0.0 < \delta < 0.6$), and size ratios ($1.2 < D_L < 1.7$). The majority of the geometric state points shown above are disorder (Dis). A Range of state points. The crystalline structures PbO, and $L_{HH}^2 K_D$ are summarized in Figure 3.8

We characterize the key crystal structure of the three main classes of crystal structures: degenerate, complete, and disordered key structures. We highlight the key crystal structures of the dimer degenerate crystalline phase ($L_H^2 K_D$), the degenerate Kagome lattice ($L_H^2 K_K$), the triangular degenerate crystal phase ($L_H^3 K_{DH}$), the elongated triangular ($L_{ET}^4 K_R$), and the disordered hexagonal ($L_H^1 K_D$). (See Figure A.1) The degenerate crystal structures have keys at the disordered center of colloidal molecule. (See Figure A.1b,d) For the complete crystal structures, both sublattices are completely ordered. (See Figure A.1c) Disordered key structures have a key sublattice that is disordered and a lock sublattice that is ordered. (See Figure A1.a, A1.e) For more details on these crystal structures and their applications, please look at Figure 2.3 and Figure 2.4 in the main text.

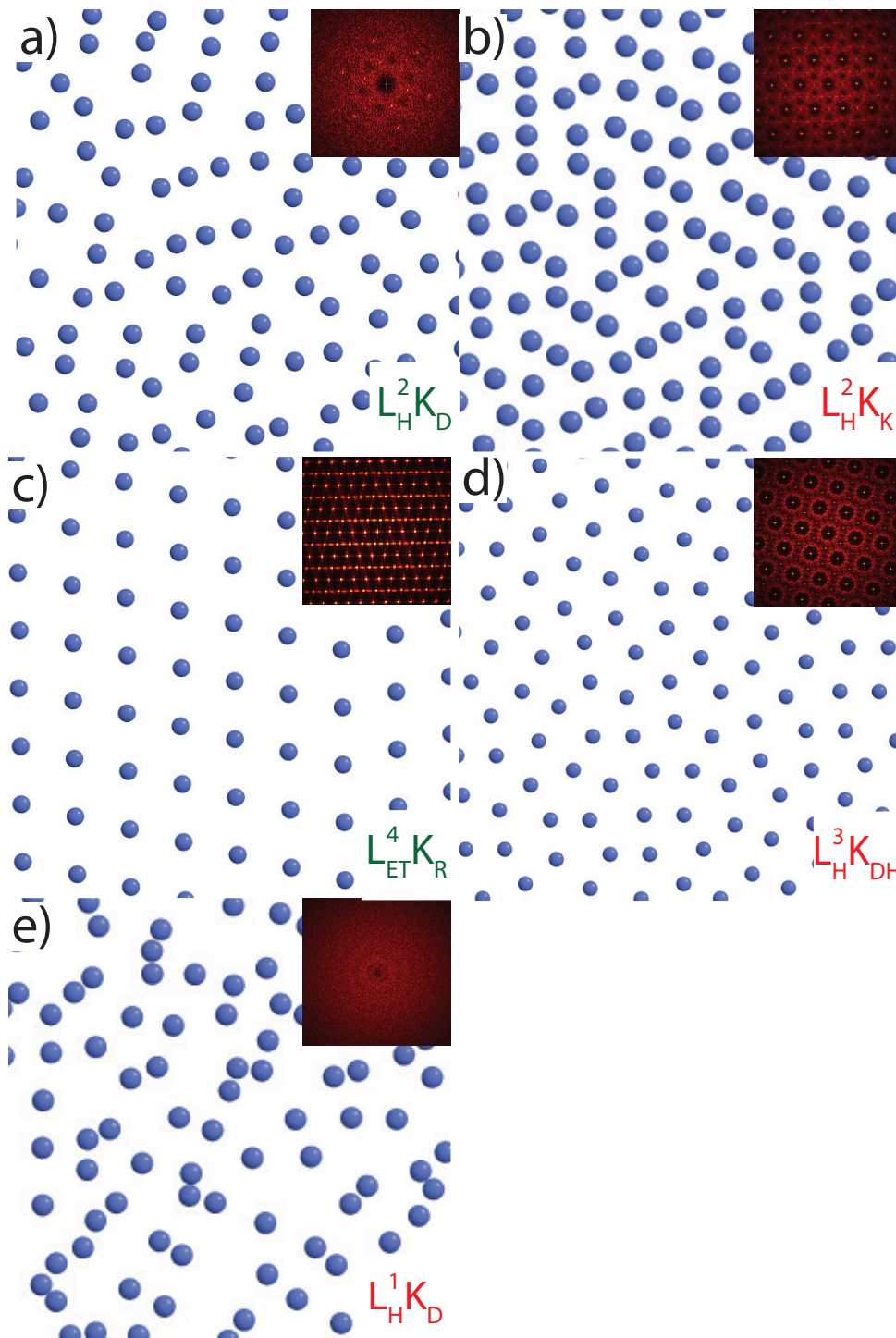


Figure A.1: The keys of the lock and key colloids are shown above. We show the keys for the (a) dimer degenerate crystalline phase ($L_H^2 K_D$), (b) degenerate Kagome lattice ($L_H^2 K_K$), (c) triangular degenerate crystal phase ($L_H^3 K_{DH}$), (d) elongated triangular ($L_{ET}^4 K_R$), (e) disordered hexagonal ($L_H^1 K_D$). An inset shows the diffraction pattern of the keys.

BIBLIOGRAPHY

BIBLIOGRAPHY

- Ajayan, P., and L. Marks (1988), Quasimelting and phases of small particles, *Physical review letters*, *60*(7), 585.
- Al-Saidi, W., H. Feng, and K. A. Fichthorn (2012), Adsorption of polyvinylpyrrolidone on ag surfaces: insight into a structure-directing agent, *Nano letters*, *12*(2), 997–1001.
- Alder, B. J., and T. Wainwright (1959), Studies in molecular dynamics. i. general method, *The Journal of Chemical Physics*, *31*, 459.
- An, J., B. Tang, X. Ning, J. Zhou, B. Zhao, W. Xu, C. Corredor, and J. R. Lombardi (2007), Photoinduced Shape Evolution: From Triangular to Hexagonal Silver Nanoplates, *The Journal of Physical Chemistry C*, *111*(49), 18,055–18,059, doi:10.1021/jp0745081.
- Anderson, J. A., and S. C. Glotzer (2013), The development and expansion of HOOMD-blue through six years of GPU proliferation.
- Anderson, J. A., C. D. Lorenz, and A. Travesset (2008), General purpose molecular dynamics simulations fully implemented on graphics processing units, *Journal of Computational Physics*, *227*(10), 5342–5359, doi:10.1016/j.jcp.2008.01.047.
- Ando, T., K. Takayanagi, K. Kobayashi, Z. Chen, Y.-M. Lin, M. J. Rooks, and P. Avouris (2007), Graphene nano-ribbon electronics, *Physica E: Low-dimensional Systems and Nanostructures*, *40*(2), 228–232.
- Ansari, M. A., and K.-Y. Kim (2007), Shape optimization of a micromixer with staggered herringbone groove, *Chemical Engineering Science*, *62*(23), 6687–6695, doi:10.1016/j.ces.2007.07.059.
- Antlanger, M., G. Doppelbauer, and G. Kahl (2011), On the stability of Archimedean tilings formed by patchy particles., *Journal of physics. Condensed matter : an Institute of Physics journal*, *23*(40), 404,206, doi:10.1088/0953-8984/23/40/404206.
- Ashton, D. J., R. L. Jack, and N. B. Wilding (2013), Self-assembly of colloidal polymers via depletion-mediated lock and key binding, *Soft Matter*, *9*, 9661–9666, doi:10.1039/C3SM51839F.
- Barrett, C. S., and T. B. Massalski (1966), *Structure of metals*, vol. 535, McGraw-Hill New York.

- Basnarkov, L., and V. Urumov (2006), Diffusion on Archimedean lattices, *Physical Review E*, *73*(4), 046,116, doi:10.1103/PhysRevE.73.046116.
- Batista, G. E., R. C. Prati, and M. C. Monard (2004), A study of the behavior of several methods for balancing machine learning training data, *ACM SIGKDD Explorations Newsletter*, *6*(1), 20–29.
- Bubeck, R., C. Bechinger, S. Nesper, and P. Leiderer (1999), Melting and reentrant freezing of two-dimensional colloidal crystals in confined geometry, *Physical review letters*, *82*(16), 3364.
- Cao, Y. C. (2004), Synthesis of square gadolinium-oxide nanoplates., *Journal of the American Chemical Society*, *126*(24), 7456–7, doi:10.1021/ja0481676.
- Chao, C., Z. Ren, S. Yin, S. Gong, X. Yang, G. Xu, X. Li, G. Shen, and G. Han (2013), Hydrothermal synthesis of ferroelectric PbTiO₃ nanoparticles with dominant {001} facets by titanate nanostructure, *CrystEngComm*, *15*(39), 8036, doi:10.1039/c3ce41248b.
- Chen, B., X. Zeng, U. Baumeister, G. Ungar, and C. Tschierske (2005), Liquid crystalline networks composed of pentagonal, square, and triangular cylinders., *Science (New York, N. Y.)*, *307*(5706), 96–9, doi:10.1126/science.1105612.
- Chen, Q., S. C. Bae, and S. Granick (2011), Directed self-assembly of a colloidal kagome lattice., *Nature*, *469*(7330), 381–4, doi:10.1038/nature09713.
- Chen, Q., S. C. Bae, and S. Granick (2012a), Staged self-assembly of colloidal metastructures, *Journal of the American Chemical Society*, *134*(27), 11,080–11,083.
- Chen, S., and D. L. Carroll (2002), Synthesis and Characterization of Truncated Triangular Silver Nanoplates, *Nano Letters*, *2*(9), 1003–1007, doi:10.1021/nl025674h.
- Chen, S., Z. Fan, and D. Carroll (2002), Silver nanodisks: synthesis, characterization, and self-assembly, *The Journal of Physical Chemistry B*.
- Chen, T., Z. Zhang, and S. C. Glotzer (2007a), Simulation studies of the self-assembly of cone-shaped particles., *Langmuir : the ACS journal of surfaces and colloids*, *23*(12), 6598–605, doi:10.1021/la063755d.
- Chen, Y., X. He, X. Zhao, Q. Yuan, and X. Gu (2007b), Preparation, characterization, and growth mechanism of a novel aligned nanosquare anatase in large quantities in the presence of TMAOH., *Journal of colloid and interface science*, *310*(1), 171–7, doi:10.1016/j.jcis.2007.01.046.
- Chen, Y., A. M. Kushner, G. A. Williams, and Z. Guan (2012b), Multiphase design of autonomic self-healing thermoplastic elastomers, *Nature Chemistry*, *4*(6), 467–472.
- Cheng, Y., M. Wang, G. Borghs, and H. Chen (2011), Gold nanoparticle dimers for plasmon sensing., *Langmuir : the ACS journal of surfaces and colloids*, *27*(12), 7884–91, doi:10.1021/la200840m.

- Cheon, J., J.-I. Park, J.-s. Choi, Y.-w. Jun, S. Kim, M. G. Kim, Y.-M. Kim, and Y. J. Kim (2006), Magnetic superlattices and their nanoscale phase transition effects., *Proceedings of the National Academy of Sciences of the United States of America*, *103*(9), 3023–7, doi:10.1073/pnas.0508877103.
- Chu, H.-C., C.-H. Kuo, and M. H. Huang (2006), Thermal aqueous solution approach for the synthesis of triangular and hexagonal gold nanoplates with three different size ranges., *Inorganic chemistry*, *45*(2), 808–13, doi:10.1021/ic051758s.
- Cohn, H., and A. Kumar (2009), Algorithmic design of self-assembling structures., *Proceedings of the National Academy of Sciences of the United States of America*, *106*(24), 9570–5, doi:10.1073/pnas.0901636106.
- Collier, C., R. Saykally, J. Shiang, S. Henrichs, and J. Heath (1997), Reversible tuning of silver quantum dot monolayers through the metal-insulator transition, *Science*, *277*(5334), 1978–1981.
- Damasceno, P. F., M. Engel, and S. C. Glotzer (2012a), Predictive self-assembly of polyhedra into complex structures., *Science (New York, N.Y.)*, *337*(6093), 453–7, doi:10.1126/science.1220869.
- Damasceno, P. F., M. Engel, and S. C. Glotzer (2012b), Crystalline assemblies and densest packings of a family of truncated tetrahedra and the role of directional entropic forces., *ACS nano*, *6*(1), 609–14, doi:10.1021/nn204012y.
- Dayal, S., M. O. Reese, A. J. Ferguson, D. S. Ginley, G. Rumbles, and N. Kopidakis (2010), The effect of nanoparticle shape on the photocarrier dynamics and photovoltaic device performance of poly (3-hexylthiophene): Cdse nanoparticle bulk heterojunction solar cells, *Advanced Functional Materials*, *20*(16), 2629–2635.
- de Vries, R. (2006), Depletion-induced instability in protein-DNA mixtures: Influence of protein charge and size., *Journal of Chemical Physics*, *125*(1), 014,905, doi: 10.1063/1.2209683.
- Demaine, E. D., and M. L. Demaine (2007), Jigsaw Puzzles, Edge Matching, and Polyomino Packing: Connections and Complexity, *Graphs and Combinatorics*, *23*(S1), 195–208, doi:10.1007/s00373-007-0713-4.
- Deng, R., F. Liang, W. Li, Z. Yang, and J. Zhu (2013), Reversible transformation of nanostructured polymer particles, *Macromolecules*, *46*(17), 7012–7017.
- Derjaguin, B. (1934), Untersuchungen über die Reibung und Adhäsion, IV, *Kolloid-Zeitschrift*, *69*(2), 155–164, doi:10.1007/BF01433225.
- Dickens, P. G., G. P. Stuttard, R. G. J. Ball, A. V. Powell, S. Hull, and S. Patat (1992), Powder neutron diffraction study of the mixed uranium?vanadium oxides Cs₂(UO₂)₂(V₂O₈) and UVO₅, *Journal of Materials Chemistry*, *2*(2), 161, doi: 10.1039/jm9920200161.

- Dickens, P. G., G. P. Stuttard, R. E. Dueber, M. J. Woodall, and S. Patat (1993), Intercalation compounds of some mixed oxides of uranium, *Solid State Ionics*, *63–65*(0), 417–423, doi:[http://dx.doi.org/10.1016/0167-2738\(93\)90138-S](http://dx.doi.org/10.1016/0167-2738(93)90138-S).
- Dijkstra, M. (1998), Phase behavior of nonadditive hard-sphere mixtures, *Physical Review E*, *58*(6), 7523–7528, doi:[10.1103/PhysRevE.58.7523](https://doi.org/10.1103/PhysRevE.58.7523).
- Dijkstra, M., R. van Roij, and R. Evans (1999), Phase diagram of highly asymmetric binary hard-sphere mixtures, *Physical Review E*, *59*(5), 5744–5771, doi:[10.1103/PhysRevE.59.5744](https://doi.org/10.1103/PhysRevE.59.5744).
- Dong, A., J. Chen, P. M. Vora, J. M. Kikkawa, and C. B. Murray (2010), Binary nanocrystal superlattice membranes self-assembled at the liquid-air interface., *Nature*, *466*(7305), 474–7, doi:[10.1038/nature09188](https://doi.org/10.1038/nature09188).
- Du, J., and R. K. O’Reilly (2011), Anisotropic particles with patchy, multicompartment and Janus architectures: preparation and application., *Chemical Society reviews*, *40*(5), 2402–16, doi:[10.1039/c0cs00216j](https://doi.org/10.1039/c0cs00216j).
- Duparcmeur, Y. (1995), Dense periodic packings of regular polygons, . . . *de Physique I*.
- Fan, F.-R., D.-Y. Liu, Y.-F. Wu, S. Duan, Z.-X. Xie, Z.-Y. Jiang, and Z.-Q. Tian (2008), Epitaxial growth of heterogeneous metal nanocrystals: From gold nanooctahedra to palladium and silver nanocubes, *Journal of the American Chemical Society*, *130*(22), 6949–6951.
- Fawcett, T., and F. Provost (1997), Adaptive fraud detection, *Data mining and knowledge discovery*, *1*(3), 291–316.
- Filion, L., and M. Dijkstra (2009), Prediction of binary hard-sphere crystal structures, *Physical Review E*, *79*(4), 046,714, doi:[10.1103/PhysRevE.79.046714](https://doi.org/10.1103/PhysRevE.79.046714).
- Fisher, D. H. (1987), Knowledge acquisition via incremental conceptual clustering, *Machine learning*, *2*(2), 139–172.
- Fjærestad, J. (2010), The 3-edge-colouring problem on the 4–8 and 3–12 lattices, *Journal of Statistical Mechanics: Theory and Experiment*, *2010*(01), P01,004.
- Florescu, M., S. Torquato, and P. J. Steinhardt (2009), Designer disordered materials with large, complete photonic band gaps, *Proceedings of the National Academy of Sciences*, *106*(49), 20,658–20,663.
- Forrest, S. R. (2004), The path to ubiquitous and low-cost organic electronic appliances on plastic, *Nature*, *428*(6986), 911–918.
- Frank, F. C., and J. S. Kasper (1958), Complex alloy structures regarded as sphere packings. I. Definitions and basic principles, *Acta Crystallographica*, *11*(3), 184–190, doi:[10.1107/S0365110X58000487](https://doi.org/10.1107/S0365110X58000487).

- Frenkel, D. (1984), Phase diagram of a system of hard ellipsoids, *Physical review . . .*
- Gilbert, E., D. Johnson, and S. Keerthi (1988), A fast procedure for computing the distance between complex objects in three-dimensional space, *IEEE Journal on Robotics and Automation*, 4(2), 193–203, doi:10.1109/56.2083.
- Glotzer, S. C. (2004), Self-Assembly of Patchy Particles, *Nano Letters*, 4(8), 1407–1413, doi:10.1021/nl0493500.
- Glotzer, S. C., and M. J. Solomon (2007), Anisotropy of building blocks and their assembly into complex structures., *Nature materials*, 6(8), 557–62, doi:10.1038/nmat1949.
- Goldberg, D. E., and J. H. Holland (1988), Genetic algorithms and machine learning, *Machine learning*, 3(2), 95–99.
- Gorkhali, S. P., J. Qi, and G. P. Crawford (2006), Switchable quasi-crystal structures with five-, seven-, and ninefold symmetries, *Journal of the Optical Society of America B*, 23(1), 149, doi:10.1364/JOSAB.23.000149.
- Greedan, J. E. (2001), Geometrically frustrated magnetic materials, *Journal of Materials Chemistry*, 11(1), 37–53, doi:10.1039/b003682j.
- Gref, R., M. Lück, P. Quellec, M. Marchand, E. Dellacherie, S. Harnisch, T. Blunk, and R. Müller (2000), ‘stealth’ corona-core nanoparticles surface modified by polyethylene glycol (peg): influences of the corona (peg chain length and surface density) and of the core composition on phagocytic uptake and plasma protein adsorption, *Colloids and Surfaces B: Biointerfaces*, 18(3–4), 301 – 313, doi: [http://dx.doi.org/10.1016/S0927-7765\(99\)00156-3](http://dx.doi.org/10.1016/S0927-7765(99)00156-3).
- Griset, A. P., J. Walpole, R. Liu, A. Gaffey, Y. L. Colson, and M. W. Grinstaff (2009), Expansile nanoparticles: synthesis, characterization, and in vivo efficacy of an acid-responsive polymeric drug delivery system, *Journal of the American Chemical Society*, 131(7), 2469–2471.
- Grünbaum, B., and G. Shephard (1977), Tilings by regular polygons, *Mathematics Magazine*.
- Grünbaum, B., and G. C. Shephard (), Tilings and patterns. 1987.
- Grünbaum, B., and G. C. Shephard (1978), The ninety-one types of isogonal tilings in the plane, *Transactions of the American Mathematical Society*, 242, 335–335, doi:10.1090/S0002-9947-1978-0496813-3.
- Grünbaum, B., and G. C. Shephard (2008), The eighty-one types of isohedral tilings in the plane, *Mathematical Proceedings of the Cambridge Philosophical Society*, 82(02), 177, doi:10.1017/S0305004100053810.

- Guo, H., Y. Chen, H. Ping, L. Wang, and D.-L. Peng (2012), One-pot synthesis of hexagonal and triangular nickel-copper alloy nanoplates and their magnetic and catalytic properties, *Journal of Materials Chemistry*, *22*(17), 8336, doi:10.1039/c2jm16095a.
- Habas, S. E., H. Lee, V. Radmilovic, G. A. Somorjai, and P. Yang (2007), Shaping binary metal nanocrystals through epitaxial seeded growth, *Nature materials*, *6*(9), 692–697.
- Haji-Akbari, A., M. Engel, A. S. Keys, X. Zheng, R. G. Petschek, P. Palffy-Muhoray, and S. C. Glotzer (2009), Disordered, quasicrystalline and crystalline phases of densely packed tetrahedra., *Nature*, *462*(7274), 773–7, doi:10.1038/nature08641.
- Harris, P. (1986), Sulphur-induced faceting of platinum catalyst particles.
- Hatton, B., L. Mishchenko, S. Davis, K. H. Sandhage, and J. Aizenberg (2010), Assembly of large-area, highly ordered, crack-free inverse opal films., *Proceedings of the National Academy of Sciences of the United States of America*, *107*(23), 10,354–9, doi:10.1073/pnas.1000954107.
- Heggen, M., L. Houben, and M. Feuerbacher (2010), Plastic-deformation mechanism in complex solids, *Nature materials*, *9*(4), 332–336.
- Henzie, J., M. Grünwald, A. Widmer-Cooper, P. L. Geissler, and P. Yang (2011), Self-assembly of uniform polyhedral silver nanocrystals into densest packings and exotic superlattices, *Nature materials*, *11*(2), 131–137.
- Hermans, T. M., M. A. C. Broeren, N. Gomopoulos, P. van der Schoot, M. H. P. van Genderen, N. A. J. M. Sommerdijk, G. Fytas, and E. W. Meijer (2009), Self-assembly of soft nanoparticles with tunable patchiness., *Nature nanotechnology*, *4*(11), 721–6, doi:10.1038/nnano.2009.232.
- Hofmeister, H., S. Nepijko, D. Ievlev, W. Schulze, and G. Ertl (2002), Composition and lattice structure of fivefold twinned nanorods of silver, *Journal of crystal growth*, *234*(4), 773–781.
- Hosein, I. D., B. S. John, S. H. Lee, F. A. Escobedo, and C. M. Liddell (2009), Rotator and crystalline films via self-assembly of short-bond-length colloidal dimers, *Journal of Materials Chemistry*, *19*(3), 344, doi:10.1039/b818613h.
- Huang, T., Q. Zhao, J. Xiao, and L. Qi (2010), Controllable self-assembly of PbS nanostars into ordered structures: close-packed arrays and patterned arrays, *ACS nano*.
- Hynninen, A.-P., C. Christova, R. van Roij, A. van Blaaderen, and M. Dijkstra (2006), Prediction and Observation of Crystal Structures of Oppositely Charged Colloids, *Physical Review Letters*, *96*(13), 138,308, doi:10.1103/PhysRevLett.96.138308.

- Iacovella, C. R., and S. C. Glotzer (2009), Complex crystal structures formed by the self-assembly of ditethered nanospheres., *Nano letters*, *9*(3), 1206–11, doi:10.1021/nl900051u.
- Iijima, S., and T. Ichihashi (1986), Structural instability of ultrafine particles of metals, *Physical review letters*, *56*(6), 616.
- Imato, K., M. Nishihara, T. Kanehara, Y. Amamoto, A. Takahara, and H. Otsuka (2012), Self-healing of chemical gels cross-linked by diarylbibenzofuranone-based trigger-free dynamic covalent bonds at room temperature, *Angewandte Chemie International Edition*, *51*(5), 1138–1142.
- Ithurria, S., M. D. Tessier, B. Mahler, R. P. S. M. Lobo, B. Dubertret, and A. L. Efros (2011), Colloidal nanoplatelets with two-dimensional electronic structure., *Nature materials*, *10*(12), 936–41, doi:10.1038/nmat3145.
- Jana, N. R., L. Gearheart, and C. J. Murphy (2001), Wet chemical synthesis of high aspect ratio cylindrical gold nanorods, *The Journal of Physical Chemistry B*, *105*(19), 4065–4067.
- Jankowski, E., and S. C. Glotzer (2012), Screening and designing patchy particles for optimized self-assembly propensity through assembly pathway engineering, *Soft Matter*, *8*(10), 2852, doi:10.1039/c2sm07101k.
- Jensen, J., and O. Sigmund (2011), Topology optimization for nano-photonics, *Laser & Photonics Reviews*, *5*(2), 308–321, doi:10.1002/lpor.201000014.
- Jin, R., Y. Cao, C. A. Mirkin, K. Kelly, G. C. Schatz, and J. Zheng (2001), Photoinduced conversion of silver nanospheres to nanoprisms, *Science*, *294*(5548), 1901–1903.
- Joshi, A. M., M. H. Tucker, W. N. Delgass, and K. T. Thomson (2006), Co adsorption on pure and binary-alloy gold clusters: A quantum chemical study, *The Journal of chemical physics*, *125*, 194,707.
- Kan, C., C. Wang, H. Li, J. Qi, J. Zhu, Z. Li, and D. Shi (2010), Gold microplates with well-defined shapes., *Small (Weinheim an der Bergstrasse, Germany)*, *6*(16), 1768–75, doi:10.1002/sml.201000600.
- Kaushik, A. P., and P. Clancy (2012), Explicit all-atom modeling of realistically sized ligand-capped nanocrystals, *Journal of Chemical Physics*, *136*(11), 114,702, doi:10.1063/1.3689973.
- Kavan, L., J.-H. Yum, and M. Grätzel (2011), Graphene nanoplatelets outperforming platinum as the electrocatalyst in co-bipyridine-mediated dye-sensitized solar cells., *Nano letters*, *11*(12), 5501–6, doi:10.1021/nl203329c.
- Kay, E. R., D. A. Leigh, and F. Zerbetto (2007), Synthetic molecular motors and mechanical machines, *Angewandte Chemie International Edition*, *46*(1-2), 72–191.

- Kepler, J. (1942), 1619, harmonices mundi, *Libri V*.
- Keys, A. S., C. R. Iacovella, and S. C. Glotzer (2011), Characterizing Structure Through Shape Matching and Applications to Self-Assembly, *Annual Review of Condensed Matter Physics*, *2*(1), 263–285, doi:10.1146/annurev-conmatphys-062910-140526.
- Khadilkar, M. R., U. Agarwal, and F. A. Escobedo (2013), Phase behavior of binary mixtures of hard convex polyhedra.
- Kim, Y., H. Han, Y. Kim, W. Lee, M. Alexe, S. Baik, and J. K. Kim (2010), Ultrahigh density array of epitaxial ferroelectric nanoislands on conducting substrates., *Nano letters*, *10*(6), 2141–6, doi:10.1021/nl100819d.
- Klajn, R., L. Fang, A. Coskun, M. A. Olson, P. J. Wesson, J. F. Stoddart, and B. A. Grzybowski (2009a), Metal nanoparticles functionalized with molecular and supramolecular switches, *Journal of the American Chemical Society*, *131*(12), 4233–4235.
- Klajn, R., M. A. Olson, P. J. Wesson, L. Fang, A. Coskun, A. Trabolsi, S. Soh, J. F. Stoddart, and B. A. Grzybowski (2009b), Dynamic hook-and-eye nanoparticle sponges, *Nature chemistry*, *1*(9), 733–738.
- Klavins, E. (2007), Programmable Self-Assembly, *IEEE Control Systems Magazine*, *27*(4), 43–56, doi:10.1109/MCS.2007.384126.
- Kohlstedt, K. L., and S. C. Glotzer (2013), Self-assembly and tunable mechanics of reconfigurable colloidal crystals, *Physical Review E*, *87*(3), 032,305, doi:10.1103/PhysRevE.87.032305.
- Koo, H., D. Yi, S. Yoo, and D.-Y. Kim (2004), A Snowman-like Array of Colloidal Dimers for Antireflecting Surfaces, *Advanced Materials*, *16*(3), 274–277, doi:10.1002/adma.200305617.
- Kowalik, M., and K. Wojciechowski (2005), Poisson’s ratio of degenerate crystalline phases of threedimensional hard dimers and hard cyclic trimers, *physica status solidi (b)*.
- Krumeich, F., M. Conrad, H.-U. Nissen, and B. Harbrecht (1998), The mesoscopic structure of disordered dodecagonal tantalum telluride: A high-resolution transmission electron microscopy study, *Philosophical Magazine Letters*, *78*(5), 357–367, doi:10.1080/095008398177751.
- Kubat, M., R. C. Holte, and S. Matwin (1998), Machine learning for the detection of oil spills in satellite radar images, *Machine learning*, *30*(2-3), 195–215.
- Kuo, K., Y. Feng, and H. Chen (1988), Growth Model of Dodecagonal Quasicrystal Based on Correlated Tiling of Squares and Equilateral Triangles, *Physical Review Letters*, *61*(15), 1740–1743, doi:10.1103/PhysRevLett.61.1740.

- Lee, G. P., A. I. Minett, P. C. Innis, and G. G. Wallace (2009), A new twist: controlled shape-shifting of silver nanoparticles from prisms to discs, *Journal of Materials Chemistry*, *19*(44), 8294–8298.
- Lee, G. P., Y. Shi, E. Lavoie, T. Daeneke, P. Reineck, U. B. Cappel, D. M. Huang, and U. Bach (2013), The light driven transformation processes of anisotropic silver nanoparticles, *ACS nano*.
- Lee, J. A., L. Meng, D. J. Norris, L. E. Scriven, and M. Tsapatsis (2006), Colloidal crystal layers of hexagonal nanoplates by convective assembly., *Langmuir : the ACS journal of surfaces and colloids*, *22*(12), 5217–9, doi:10.1021/la0601206.
- Leong, T. G., P. A. Lester, T. L. Koh, E. K. Call, and D. H. Gracias (2007a), Surface tension-driven self-folding polyhedra., *Langmuir : the ACS journal of surfaces and colloids*, *23*(17), 8747–51, doi:10.1021/la700913m.
- Leong, T. G., P. A. Lester, T. L. Koh, E. K. Call, and D. H. Gracias (2007b), Surface tension-driven self-folding polyhedra, *Langmuir*, *23*(17), 8747–8751.
- Leunissen, M. E., C. G. Christova, A.-P. Hynninen, C. P. Royall, A. I. Campbell, A. Imhof, M. Dijkstra, R. van Roij, and A. van Blaaderen (2005), Ionic colloidal crystals of oppositely charged particles., *Nature*, *437*(7056), 235–40, doi:10.1038/nature03946.
- Li, F., W. C. Yoo, M. B. Beernink, and A. Stein (2009a), Site-specific functionalization of anisotropic nanoparticles: from colloidal atoms to colloidal molecules., *Journal of the American Chemical Society*, *131*(51), 18,548–55, doi:10.1021/ja908364k.
- Li, H., M. Eddaoudi, M. O’Keeffe, and O. M. Yaghi (1999), Design and synthesis of an exceptionally stable and highly porous metal-organic framework, *402*(6759), 276–279, doi:10.1038/46248.
- Li, M., L. Xu, C. Sun, Z. Ju, and Y. Qian (2009b), Thermal-induced shape evolution from uniform triangular to hexagonal r-BN nanoplates, *Journal of Materials Chemistry*, *19*(43), 8086, doi:10.1039/b912451a.
- Li, S.-S., H.-J. Yan, L.-J. Wan, H.-B. Yang, B. H. Northrop, and P. J. Stang (2007), Control of supramolecular rectangle self-assembly with a molecular template., *Journal of the American Chemical Society*, *129*(30), 9268–9, doi:10.1021/ja0733282.
- Li, X., H. Shen, J. Niu, S. Li, Y. Zhang, H. Wang, and L. S. Li (2010), Columnar self-assembly of Cu₂S hexagonal nanoplates induced by tin(IV)-X complex as inorganic surface ligand., *Journal of the American Chemical Society*, *132*(37), 12,778–9, doi:10.1021/ja103955s.
- Liddell, C., and C. Summers (2003), Monodispersed ZnS Dimers, Trimers, and Tetramers for Lower Symmetry Photonic Crystal Lattices, *Advanced Materials*, *15*(20), 1715–1719, doi:10.1002/adma.200305283.

- Liu, B., and D. Wang (2012), High-throughput transformation of colloidal polymer spheres to discs simply via magnetic stirring of their dispersions, *Langmuir*, *28*(15), 6436–6440.
- Liu, Y., W. Li, T. Perez, J. D. Gunton, and G. Brett (2012a), Self assembly of Janus ellipsoids., *Langmuir : the ACS journal of surfaces and colloids*, *28*(1), 3–9, doi:10.1021/la2032303.
- Liu, Z., H. Zhou, Y. S. Lim, J.-H. Song, L. Piao, and S.-H. Kim (2012b), Synthesis of silver nanoplates by two-dimensional oriented attachment, *Langmuir*, *28*(25), 9244–9249.
- Lu, L., A. Kobayashi, K. Tawa, and Y. Ozaki (2006), Silver Nanoplates with Special Shapes: Controlled Synthesis and Their Surface Plasmon Resonance and Surface-Enhanced Raman Scattering Properties, *Chemistry of Materials*, *18*(20), 4894–4901, doi:10.1021/cm0615875.
- Man, W., M. Megens, P. J. Steinhardt, and P. M. Chaikin (2005), Experimental measurement of the photonic properties of icosahedral quasicrystals., *Nature*, *436*(7053), 993–6, doi:10.1038/nature03977.
- Mannoor, M. S., Z. Jiang, T. James, Y. L. Kong, K. A. Malatesta, W. O. Soboyejo, N. Verma, D. H. Gracias, and M. C. McAlpine (2013), 3D Printed Bionic Ears., *Nano letters*, *13*(6), 2634–2639, doi:10.1021/nl4007744.
- Marchetti, M. C. (2012), Active matter: Spontaneous flows and self-propelled drops., *Nature*, *491*(7424), 340–1, doi:10.1038/nature11750.
- Maye, M. M., M. T. Kumara, D. Nykypanchuk, W. B. Sherman, and O. Gang (2010), Switching binary states of nanoparticle superlattices and dimer clusters by DNA strands., *Nature nanotechnology*, *5*(2), 116–20, doi:10.1038/nnano.2009.378.
- McCandlish, S. R., A. Baskaran, and M. F. Hagan (2012), Spontaneous segregation of self-propelled particles with different motilities, *Soft Matter*, *8*(8), 2527, doi:10.1039/c2sm06960a.
- McConnell, M. D., M. J. Kraeutler, S. Yang, and R. J. Composto (2010), Patchy and multiregion janus particles with tunable optical properties., *Nano letters*, *10*(2), 603–9, doi:10.1021/nl903636r.
- McMahon, M., O. Degtyareva, and R. Nemes (2000), Ba-iv-type incommensurate crystal structure in group-v metals, *Physical Review Letters*, *85*(23), 4896.
- Medintz, I. L., H. T. Uyeda, E. R. Goldman, and H. Mattoussi (2005), Quantum dot bioconjugates for imaging, labelling and sensing, *Nature materials*, *4*(6), 435–446.
- Merz, L., M. Parschau, J. S. Siegel, and K.-H. Ernst (2009), Condensation of Fivefold-Symmetric Molecules in Two Dimensions, *CHIMIA International Journal for Chemistry*, *63*(4), 214–216, doi:10.2533/chimia.2009.214.

- Metropolis, N., and S. Ulam (1949), The monte carlo method, *Journal of the American statistical association*, *44*(247), 335–341.
- Mikhael, J., J. Roth, L. Helden, and C. Bechinger (2008), Archimedean-like tiling on decagonal quasicrystalline surfaces., *Nature*, *454*(7203), 501–4, doi:10.1038/nature07074.
- Milinković, K., M. Dennison, and M. Dijkstra (2013), Phase diagram of hard asymmetric dumbbell particles, *Physical Review E*, *87*(3), 032,128, doi:10.1103/PhysRevE.87.032128.
- Miszta, K., et al. (2011), Hierarchical self-assembly of suspended branched colloidal nanocrystals into superlattice structures., *Nature materials*, *10*(11), 872–6, doi:10.1038/nmat3121.
- Mitragotri, S., and J. Lahann (2009), Physical approaches to biomaterial design., *Nature materials*, *8*(1), 15–23, doi:10.1038/nmat2344.
- Mohammadi, B., and O. Pironneau (2004), SHAPE OPTIMIZATION IN FLUID MECHANICS, *Annual Review of Fluid Mechanics*, *36*(1), 255–279, doi:10.1146/annurev.fluid.36.050802.121926.
- Möller, S., C. Perlov, W. Jackson, C. Taussig, and S. R. Forrest (2003), A polymer/semiconductor write-once read-many-times memory, *Nature*, *426*(6963), 166–169.
- Mostafa, S., F. Behafarid, J. R. Croy, L. K. Ono, L. Li, J. C. Yang, A. I. Frenkel, and B. R. Cuenya (2010), Shape-dependent catalytic properties of pt nanoparticles, *Journal of the American Chemical Society*, *132*(44), 15,714–15,719.
- Motornov, M., R. Sheparovych, R. Lupitskyy, E. MacWilliams, O. Hoy, I. Luzinov, and S. Minko (2007), Stimuli-responsive colloidal systems from mixed brush-coated nanoparticles, *Advanced Functional Materials*, *17*(14), 2307–2314.
- Murphy, C. J., A. M. Gole, S. E. Hunyadi, and C. J. Orendorff (2006), One-dimensional colloidal gold and silver nanostructures, *Inorganic chemistry*, *45*(19), 7544–7554.
- Narayanan, R., and M. A. El-Sayed (2005), Catalysis with transition metal nanoparticles in colloidal solution: nanoparticle shape dependence and stability., *The journal of physical chemistry. B*, *109*(26), 12,663–76, doi:10.1021/jp051066p.
- Nelson, D. (1983), Order, frustration, and defects in liquids and glasses, *Physical review B*.
- Nguyen, N. H. P., E. Jankowski, and S. C. Glotzer (2012), Thermal and athermal three-dimensional swarms of self-propelled particles, *Physical Review E*, *86*(1), 011,136, doi:10.1103/PhysRevE.86.011136.

- Nguyen, T. D., E. Jankowski, and S. C. Glotzer (2011), Self-assembly and re-configurability of shape-shifting particles., *ACS nano*, 5(11), 8892–903, doi:10.1021/nm203067y.
- Nikoobakht, B., and M. A. El-Sayed (2003), Preparation and Growth Mechanism of Gold Nanorods (NRs) Using Seed-Mediated Growth Method, *Chemistry of Materials*, 15(10), 1957–1962, doi:10.1021/cm020732l.
- Nykypanchuk, D., M. M. Maye, D. van der Lelie, and O. Gang (2008), DNA-guided crystallization of colloidal nanoparticles., *Nature*, 451(7178), 549–52, doi:10.1038/nature06560.
- O’Keeffe, M., and B. Hyde (1980), Plane nets in crystal chemistry, *Philosophical Transactions of the Royal Society of London. Series A, Mathematical and Physical Sciences*, pp. 553–618.
- Paik, T., and C. Murray (2013), Shape-Directed Binary Assembly of Anisotropic Nanoplates: A Nanocrystal Puzzle with Shape-Complementary Building Blocks, *Nano letters*.
- Paik, T., D.-K. Ko, T. R. Gordon, V. Doan-Nguyen, and C. B. Murray (2011), Studies of liquid crystalline self-assembly of GdF nanoplates by in-plane, out-of-plane SAXS., *ACS nano*, 5(10), 8322–30, doi:10.1021/nm203049t.
- Paik, T., T. R. Gordon, A. M. Prantner, H. Yun, and C. B. Murray (2013), Designing Tripodal and Triangular Gadolinium Oxide Nanoplates and Self-Assembled Nanofibrils as Potential Multimodal Bioimaging Probes., *ACS nano*, doi:10.1021/nm4004583.
- Pal, S., Y. K. Tak, and J. M. Song (2007), Does the antibacterial activity of silver nanoparticles depend on the shape of the nanoparticle? A study of the Gram-negative bacterium *Escherichia coli*., *Applied and environmental microbiology*, 73(6), 1712–20, doi:10.1128/AEM.02218-06.
- Park, K. H., K. Jang, and S. U. Son (2006), Synthesis, Optical Properties, and Self-Assembly of Ultrathin Hexagonal In₂S₃ Nanoplates, *Angewandte Chemie*, 118(28), 4724–4728, doi:10.1002/ange.200601031.
- Park, M., et al. (2011), Large-Scale Synthesis of Ultrathin Manganese Oxide Nanoplates and Their Applications to T1 MRI Contrast Agents, *Chemistry of Materials*, 23(14), 3318–3324, doi:10.1021/cm200414c.
- Pawar, A. B., and I. Kretzschmar (2010), Fabrication, assembly, and application of patchy particles, *Macromolecular rapid communications*, 31(2), 150–168.
- Phan, S.-E., W. B. Russel, J. Zhu, and P. M. Chaikin (1998), Effects of polydispersity on hard sphere crystals, *The Journal of Chemical Physics*, 108(23), 9789, doi:10.1063/1.476453.

- Phillips, C. L., E. Jankowski, M. Marval, and S. C. Glotzer (2012), Self-assembled clusters of spheres related to spherical codes, *Physical Review E*, *86*(4), 041,124.
- Plimpton, S. (1995), Fast Parallel Algorithms for Short-Range Molecular Dynamics, *Journal of Computational Physics*, *117*(1), 1–19, doi:10.1006/jcph.1995.1039.
- Podsiadlo, P., G. V. Krylova, A. Demortière, and E. V. Shevchenko (2010), Multi-component periodic nanoparticle superlattices, *Journal of Nanoparticle Research*, *13*(1), 15–32, doi:10.1007/s11051-010-0174-1.
- Porel, S., S. Singh, and T. P. Radhakrishnan (2005), Polygonal gold nanoplates in a polymer matrix., *Chemical communications (Cambridge, England)*, (18), 2387–9, doi:10.1039/b500536a.
- Pradhan, M., S. Sarkar, A. K. Sinha, M. Basu, and T. Pal (2011), Morphology controlled uranium oxide hydroxide hydrate for catalysis, luminescence and SERS studies, *CrystEngComm*, *13*(8), 2878, doi:10.1039/c0ce00666a.
- Qi, W., J. d. Graaf, F. Qiao, S. Marras, L. Manna, and M. Dijkstra (2012), Ordered two-dimensional superstructures of colloidal octapod-shaped nanocrystals on flat substrates, *Nano letters*, *12*(10), 5299–5303.
- REILING, G. H. (1964), Characteristics of Mercury Vapor-Metallic Iodide Arc Lamps, *Journal of the Optical Society of America*, *54*(4), 532, doi:10.1364/JOSA.54.000532.
- Ressouche, E., V. Simonet, B. Canals, M. Gospodinov, and V. Skumryev (2009), Magnetic Frustration in an Iron-Based Cairo Pentagonal Lattice, *Physical Review Letters*, *103*(26), 267,204, doi:10.1103/PhysRevLett.103.267204.
- Ross, B. M., L. Y. Wu, and L. P. Lee (2011), Omnidirectional 3d nanoplasmonic optical antenna array via soft-matter transformation, *Nano letters*, *11*(7), 2590–2595.
- Rüegg, A., and G. A. Fiete (2011), Topological insulators from complex orbital order in transition-metal oxides heterostructures, *Physical Review B*, *84*(20), 201,103, doi:10.1103/PhysRevB.84.201103.
- Ryckaert, J.-P., G. Ciccotti, and H. J. Berendsen (1977), Numerical integration of the cartesian equations of motion of a system with constraints: molecular dynamics of n-alkanes, *Journal of Computational Physics*, *23*(3), 327–341, doi:10.1016/0021-9991(77)90098-5.
- Sacanna, S., W. T. M. Irvine, P. M. Chaikin, and D. J. Pine (2010), Lock and key colloids., *Nature*, *464*(7288), 575–8, doi:10.1038/nature08906.
- Salazar-Alvarez, G., et al. (2008), Cubic versus spherical magnetic nanoparticles: the role of surface anisotropy, *Journal of the American Chemical Society*, *130*(40), 13,234–13,239.

- Sau, T., and C. Murphy (2007), Role of ions in the colloidal synthesis of gold nanowires, *Philosophical Magazine*, *87*(14-15), 2143–2158.
- Sau, T. K., and C. J. Murphy (2004), Seeded high yield synthesis of short Au nanorods in aqueous solution., *Langmuir : the ACS journal of surfaces and colloids*, *20*(15), 6414–20, doi:10.1021/la049463z.
- Sau, T. K., and C. J. Murphy (2005), Self-Assembly Patterns Formed upon Solvent Evaporation of Aqueous Cetyltrimethylammonium Bromide-Coated Gold Nanoparticles of Various Shapes, *Langmuir*, *21*(7), 2923–2929, doi:10.1021/la047488s.
- Schapotschnikow, P., R. Pool, and T. J. H. Vlugt (2008), Molecular simulations of interacting nanocrystals, *Nano Letters*, *8*(9), 2930–2934, doi:10.1021/nl8017862.
- Schlickum, U., et al. (2008), Chiral kagomé lattice from simple ditopic molecular bricks, *Journal of the American Chemical Society*, *130*(35), 11,778–11,782.
- Sciortino, F., and E. Zaccarelli (2011), Reversible gels of patchy particles, *Current Opinion in Solid State and Materials Science*, *15*(6), 246–253, doi:10.1016/j.cossms.2011.07.003.
- Shen, H., H. Wang, H. Yuan, L. Ma, and L. S. Li (2012a), Size-, shape-, and assembly-controlled synthesis of Cu₂xSe nanocrystals via a non-injection phosphine-free colloidal method, *CrystEngComm*, *14*(2), 555, doi:10.1039/c1ce05887h.
- Shen, H., H. Wang, H. Yuan, L. Ma, and L. S. Li (2012b), Size-, shape-, and assembly-controlled synthesis of Cu₂xSe nanocrystals via a non-injection phosphine-free colloidal method, *CrystEngComm*, *14*(2), 555, doi:10.1039/c1ce05887h.
- Sheng, H., W. Luo, F. Alamgir, J. Bai, and E. Ma (2006), Atomic packing and short-to-medium-range order in metallic glasses, *Nature*, *439*(7075), 419–425.
- Shevchenko, E. V., D. V. Talapin, N. A. Kotov, S. O’Brien, and C. B. Murray (2006), Structural diversity in binary nanoparticle superlattices., *Nature*, *439*(7072), 55–9, doi:10.1038/nature04414.
- Shevchenko, E. V., M. Ringler, A. Schwemer, D. V. Talapin, T. A. Klar, A. L. Rogach, J. Feldmann, and A. P. Alivisatos (2008), Self-assembled binary superlattices of CdSe and Au nanocrystals and their fluorescence properties., *Journal of the American Chemical Society*, *130*(11), 3274–5, doi:10.1021/ja710619s.
- Smrdel, P., M. Bogataj, A. Zega, O. Planinšek, and A. Mrhar (2008), Shape optimization and characterization of polysaccharide beads prepared by ionotropic gelation.
- Sobieszczanski-Sobieski, J., and R. T. Haftka (1997), Multidisciplinary aerospace design optimization: survey of recent developments, *Structural Optimization*, *14*(1), 1–23, doi:10.1007/BF01197554.

- Sokolowski, J., and J.-P. Zolesio (1992), *Introduction to Shape Optimization, Springer Series in Computational Mathematics*, vol. 16, Springer Berlin Heidelberg, Berlin, Heidelberg, doi:10.1007/978-3-642-58106-9.
- Solomon, M. J., R. Zeitoun, D. Ortiz, K. E. Sung, D. Deng, A. Shah, M. A. Burns, S. C. Glotzer, and J. M. Millunchick (2010), Toward Assembly of Non-close-packed Colloidal Structures from Anisotropic Pentamer Particles., *Macromolecular rapid communications*, *31*(2), 196–201, doi:10.1002/marc.200900586.
- Srivastava, S., et al. (2010), Light-controlled self-assembly of semiconductor nanoparticles into twisted ribbons, *Science*, *327*(5971), 1355–1359.
- Stampfli, P. (1986), A dodecagonal quasiperiodic lattice in two dimensions, *Helv. Phys. Acta*.
- Su, X., F. Xiao, Y. Li, J. Jian, Q. Sun, and J. Wang (2010), Synthesis of uniform WO₃ square nanoplates via an organic acid-assisted hydrothermal process, *Materials Letters*, *64*(10), 1232–1234, doi:http://dx.doi.org/10.1016/j.matlet.2010.02.063.
- Sun, Y., and Y. Xia (2002), Shape-Controlled Synthesis of Gold and Silver Nanoparticles , *Science*, *298*(5601), 2176–2179, doi:10.1126/science.1077229.
- Sun, Y., and Y. Xia (2003), Triangular Nanoplates of Silver: Synthesis, Characterization, and Use as Sacrificial Templates For Generating Triangular Nanorings of Gold, *Advanced Materials*, *15*(9), 695–699, doi:10.1002/adma.200304652.
- Sun, Y., B. Mayers, and Y. Xia (2003), Transformation of silver nanospheres into nanobelts and triangular nanoplates through a thermal process, *Nano Letters*, *3*(5), 675–679.
- Tahara, K., et al. (2006), Two-dimensional porous molecular networks of dehydrobenzo [12] annulene derivatives via alkyl chain interdigitation, *Journal of the American Chemical Society*, *128*(51), 16,613–16,625.
- Takano, A., W. Kawashima, A. Noro, Y. Isono, N. Tanaka, T. Dotera, and Y. Matsushita (2005), A mesoscopic Archimedean tiling having a new complexity in an ABC star polymer, *Journal of Polymer Science Part B: Polymer Physics*, *43*(18), 2427–2432, doi:10.1002/polb.20537.
- Talapin, D. V., E. V. Shevchenko, M. I. Bodnarchuk, X. Ye, J. Chen, and C. B. Murray (2009), Quasicrystalline order in self-assembled binary nanoparticle superlattices., *Nature*, *461*(7266), 964–7, doi:10.1038/nature08439.
- Tam, E., P. Podsiadlo, E. Shevchenko, D. F. Ogletree, M.-P. Delplancke-Ogletree, and P. D. Ashby (2010), Mechanical properties of face-centered cubic supercrystals of nanocrystals, *Nano letters*, *10*(7), 2363–2367.

- Tang, B., S. Xu, J. An, B. Zhao, and W. Xu (2009), Photoinduced Shape Conversion and Reconstruction of Silver Nanoprisms, *The Journal of Physical Chemistry C*, *113*(17), 7025–7030, doi:10.1021/jp810711a.
- Tao, A., P. Sinsersuksakul, and P. Yang (2006), Polyhedral silver nanocrystals with distinct scattering signatures, *Angewandte Chemie International Edition*, *45*(28), 4597–4601.
- Tao, A. R., S. Habas, and P. Yang (2008), Shape Control of Colloidal Metal Nanocrystals, *Small*, *4*(3), 310–325, doi:10.1002/sml.200701295.
- Tao, Y., Y. Shen, L. Yang, B. Han, F. Huang, S. Li, Z. Chu, and A. Xie (2012), Hierarchical self-assembly of hexagonal single-crystal nanosheets into 3D layered superlattices with high conductivity., *Nanoscale*, *4*(12), 3729–33, doi:10.1039/c2nr30743j.
- Teranishi, T., and M. Miyake (1998), Size control of palladium nanoparticles and their crystal structures, *Chemistry of materials*, *10*(2), 594–600.
- Topping, B. H. V. (1983), Shape Optimization of Skeletal Structures: A Review, *Journal of Structural Engineering*, *109*(8), 1933–1951, doi:10.1061/(ASCE)0733-9445(1983)109:8(1933).
- Torquato, S. (2009), Inverse optimization techniques for targeted self-assembly, *Soft Matter*, *5*(6), 1157, doi:10.1039/b814211b.
- Tsuiji, M., X. Tang, M. Matsunaga, Y. Maeda, and M. Watanabe (2010), Shape Evolution of Flag Types of Silver Nanostructures from Nanorod Seeds in PVP-Assisted DMF Solution, *Crystal Growth & Design*, *10*(12), 5238–5243, doi:10.1021/cg101041m.
- Ueda, K., T. Dotera, and T. Gemma (2007), Photonic band structure calculations of two-dimensional Archimedean tiling patterns, *Physical Review B*, *75*(19), 195,122, doi:10.1103/PhysRevB.75.195122.
- Umar, A. A., M. Oyama, M. M. Salleh, and B. Y. Majlis (2009), Formation of High-Yield Gold Nanoplates on the Surface: Effective Two-Dimensional Crystal Growth of Nanoseed in the Presence of Poly(vinylpyrrolidone) and Cetyltrimethylammonium Bromide, *Crystal Growth & Design*, *9*(6), 2835–2840, doi:10.1021/cg900109x.
- Urban, J. J., D. V. Talapin, E. V. Shevchenko, C. R. Kagan, and C. B. Murray (2007), Synergism in binary nanocrystal superlattices leads to enhanced p-type conductivity in self-assembled PbTe/Ag₂Te thin films., *Nature materials*, *6*(2), 115–21, doi:10.1038/nmat1826.
- Vácha, R., and D. Frenkel (2013), Simulations Suggest Possible Novel Membrane Pore Structure., *Langmuir : the ACS journal of surfaces and colloids*, doi:10.1021/la402727a.

- van Anders, G., N. K. Ahmed, D. Klotsa, M. Engel, and S. C. Glotzer (2013a), Unified Theoretical Framework for Shape Entropy in Colloids.
- van Anders, G., N. K. Ahmed, D. Klotsa, M. Engel, and S. C. Glotzer (2013b), Unified Theoretical Framework for Shape Entropy in Colloids.
- van Anders, G., N. K. Ahmed, R. Smith, M. Engel, and S. C. Glotzer (2013c), Entropically Patchy Particles.
- van Blaaderen, A. (2006), Materials Science: colloids get complex., *Nature*, *439*(7076), 545–6, doi:10.1038/439545a.
- van der Linden, M. N., J. P. K. Doye, and A. A. Louis (2012), Formation of dodecagonal quasicrystals in two-dimensional systems of patchy particles., *The Journal of chemical physics*, *136*(5), 054,904, doi:10.1063/1.3679653.
- Van Dillen, T., E. Snoeks, W. Fukarek, C. van Kats, K. Velikov, A. van Blaaderen, and A. Polman (2001), Anisotropic deformation of colloidal particles under mev ion irradiation, *Nuclear Instruments and Methods in Physics Research Section B: Beam Interactions with Materials and Atoms*, *175*, 350–356.
- van Huis, M. A., A. Figuerola, C. Fang, A. Béché, H. W. Zandbergen, and L. Manna (2011), Chemical transformation of au-tipped cds nanorods into aus/cd core/shell particles by electron beam irradiation, *Nano letters*, *11*(11), 4555–4561.
- van Oers, M. C., F. P. Rutjes, and J. C. van Hest (2013), Tubular polymersomes: a crosslinker-induced shape transformation, *Journal of the American Chemical Society*.
- Veerman, J., and D. Frenkel (1990), Phase diagram of a system of hard spherocylinders by computer simulation, *Physical Review A: atomic,*
- Velikov, K. P., T. van Dillen, A. Polman, and A. van Blaaderen (2002), Photonic crystals of shape-anisotropic colloidal particles, *Applied physics letters*, *81*(5), 838–840.
- Verma, A., and F. Stellacci (2010), Effect of surface properties on nanoparticle–cell interactions, *Small*, *6*(1), 12–21, doi:10.1002/smll.200901158.
- Vestal, C. R., and Z. J. Zhang (2003), Effects of surface coordination chemistry on the magnetic properties of mnfe₂o₄ spinel ferrite nanoparticles, *Journal of the American Chemical Society*, *125*(32), 9828–9833, doi:10.1021/ja035474n.
- Viarbitskaya, S., A. Teulle, R. Marty, J. Sharma, C. Girard, A. Arbouet, and E. Du-jardin (2013), Tailoring and imaging the plasmonic local density of states in crystalline nanoprisms., *Nature materials*, *12*(5), 426–32, doi:10.1038/nmat3581.
- Vlassiuk, I., C.-D. Park, S. A. Vail, D. Gust, and S. Smirnov (2006), Control of nanopore wetting by a photochromic spiropyran: A light-controlled valve and electrical switch, *Nano letters*, *6*(5), 1013–1017.

- VON BRECHT, J. H., D. UMINSKY, T. KOLOKOLNIKOV, and A. L. BERTOZZI (2012), PREDICTING PATTERN FORMATION IN PARTICLE INTERACTIONS, *Mathematical Models and Methods in Applied Sciences*, 22(supp01), 1140,002, doi:10.1142/S0218202511400021.
- Wagner, R., and W. Ellis (1964), Vapor-liquid-solid mechanism of single crystal growth, *Applied Physics Letters*, 4(5), 89–90.
- Wang, F., and Y. Ran (2011), Nearly flat band with Chern number $C=2$ on the dice lattice, *Physical Review B*, 84(24), 241,103, doi:10.1103/PhysRevB.84.241103.
- Wang, H., H. S. Casalongue, Y. Liang, and H. Dai (2010), Ni(OH)₂ nanoplates grown on graphene as advanced electrochemical pseudocapacitor materials., *Journal of the American Chemical Society*, 132(21), 7472–7, doi:10.1021/ja102267j.
- Wang, Y., Y. Wang, D. R. Breed, V. N. Manoharan, L. Feng, A. D. Hollingsworth, M. Weck, and D. J. Pine (2012), Colloids with valence and specific directional bonding., *Nature*, 491(7422), 51–5, doi:10.1038/nature11564.
- Whitelam, S., I. Tamblyn, P. H. Beton, and J. P. Garrahan (2012), Random and Ordered Phases of Off-Lattice Rhombus Tiles, *Physical Review Letters*, 108(3), 035,702, doi:10.1103/PhysRevLett.108.035702.
- Whitesides, G. M., and B. Grzybowski (2002), Self-assembly at all scales, *Science*, 295(5564), 2418–2421.
- Wiley, B. J., S. H. Im, Z.-Y. Li, J. McLellan, A. Siekkinen, and Y. Xia (2006a), Maneuvering the surface plasmon resonance of silver nanostructures through shape-controlled synthesis., *The journal of physical chemistry. B*, 110(32), 15,666–75, doi:10.1021/jp0608628.
- Wiley, B. J., S. H. Im, Z.-Y. Li, J. McLellan, A. Siekkinen, and Y. Xia (2006b), Maneuvering the surface plasmon resonance of silver nanostructures through shape-controlled synthesis., *The journal of physical chemistry. B*, 110(32), 15,666–75, doi:10.1021/jp0608628.
- Wojciechowski, K. (1992), Monte Carlo simulations of highly anisotropic two-dimensional hard dumbbell-shaped molecules: Nonperiodic phase between fluid and dense solid, *Physical Review B*, 46(1), 26–39, doi:10.1103/PhysRevB.46.26.
- Wojciechowski, K., and D. Frenkel (2004), Tetratic phase in the planar hard square system?, *Computational Methods in . . .*
- Xi, G., and J. Ye (2010), Synthesis of bismuth vanadate nanoplates with exposed {001} facets and enhanced visible-light photocatalytic properties., *Chemical communications (Cambridge, England)*, 46(11), 1893–5, doi:10.1039/b923435g.
- Xia, F., et al. (2008), Gating of single synthetic nanopores by proton-driven dna molecular motors, *Journal of the American Chemical Society*, 130(26), 8345–8350.

- Xia, Y., Y. Xiong, B. Lim, and S. E. Skrabalak (2009a), Shape-controlled synthesis of metal nanocrystals: simple chemistry meets complex physics?, *Angewandte Chemie (International ed. in English)*, *48*(1), 60–103, doi:10.1002/anie.200802248.
- Xia, Y., Y. Xiong, B. Lim, and S. E. Skrabalak (2009b), Shape-controlled synthesis of metal nanocrystals: Simple chemistry meets complex physics?, *Angewandte Chemie International Edition*, *48*(1), 60–103.
- Xiong, Y., J. M. McLellan, J. Chen, Y. Yin, Z.-Y. Li, and Y. Xia (2005), Kinetically controlled synthesis of triangular and hexagonal nanoplates of palladium and their SPR/SERS properties., *Journal of the American Chemical Society*, *127*(48), 17,118–27, doi:10.1021/ja056498s.
- Xiu, Z.-M., J. Ma, and P. J. Alvarez (2011), Differential effect of common ligands and molecular oxygen on antimicrobial activity of silver nanoparticles versus silver ions, *Environmental science & technology*, *45*(20), 9003–9008.
- Xu, F., Z.-Y. Yuan, G.-H. Du, M. Halasa, and B.-L. Su (2006), High-yield synthesis of single-crystalline ZnO hexagonal nanoplates and accounts of their optical and photocatalytic properties, *Applied Physics A*, *86*(2), 181–185, doi:10.1007/s00339-006-3745-3.
- Yang, Y., S. Matsubara, L. Xiong, T. Hayakawa, and M. Nogami (2007), Solvothermal Synthesis of Multiple Shapes of Silver Nanoparticles and Their SERS Properties, *Journal of Physical Chemistry C*, *111*(26), 9095–9104, doi:10.1021/jp068859b.
- Ye, X., J. E. Collins, Y. Kang, J. Chen, D. T. N. Chen, A. G. Yodh, and C. B. Murray (2010), Morphologically controlled synthesis of colloidal upconversion nanophosphors and their shape-directed self-assembly., *Proceedings of the National Academy of Sciences of the United States of America*, *107*(52), 22,430–5, doi:10.1073/pnas.1008958107.
- Ye, X., J. A. Millan, M. Engel, J. Chen, B. T. Diroll, S. C. Glotzer, and C. B. Murray (2013a), Shape alloys of nanorods and nanospheres from self-assembly, *Nano letters*, *13*(10), 4980–4988.
- Ye, X., et al. (2013b), Competition of shape and interaction patchiness for self-assembling nanoplates., *Nature chemistry*, *5*(6), 466–73, doi:10.1038/nchem.1651.
- Ye, X., et al. (2013c), Competition of shape and interaction patchiness for self-assembling nanoplates, *Nature Chemistry*, *5*(6), 466–473, doi:10.1038/nchem.1651.
- Zachary, C. E., and S. Torquato (2009), Hyperuniformity in point patterns and two-phase random heterogeneous media, *Journal of Statistical Mechanics: Theory and Experiment*, *2009*(12), P12,015.
- Zeng, Y., H. Li, B. Xiang, H. Ma, B. Qu, M. Xia, Y. Wang, Q. Zhang, and Y. Wang (2010), Synthesis and characterization of phase-purity Cu₉BiS₆ nanoplates, *Materials Letters*, *64*(9), 1091–1094, doi:10.1016/j.matlet.2010.02.022.

- Zhang, C., and Y. Zhu (2005), Synthesis of Square Bi₂WO₆ Nanoplates as High-Activity Visible-Light-Driven Photocatalysts, *Chemistry of Materials*, *17*(13), 3537–3545, doi:10.1021/cm0501517.
- Zhang, F., Y. Liu, and H. Yan (2013), Complex Archimedean tiling self-assembled from DNA nanostructures., *Journal of the American Chemical Society*, *135*(20), 7458–61, doi:10.1021/ja4035957.
- Zhang, J., M. R. Langille, and C. A. Mirkin (2011a), Synthesis of silver nanorods by low energy excitation of spherical plasmonic seeds, *Nano letters*, *11*(6), 2495–2498.
- Zhang, J.-T., L. Wang, J. Luo, A. Tikhonov, N. Kornienko, and S. A. Asher (2011b), 2-D array photonic crystal sensing motif., *Journal of the American Chemical Society*, *133*(24), 9152–5, doi:10.1021/ja201015c.
- Zhang, Q., J. Ge, T. Pham, J. Goebel, Y. Hu, Z. Lu, and Y. Yin (2009), Reconstruction of silver nanoplates by uv irradiation: tailored optical properties and enhanced stability, *Angewandte Chemie*, *121*(19), 3568–3571.
- Zhang, Y., F. Lu, D. van der Lelie, and O. Gang (2011c), Continuous phase transformation in nanocube assemblies, *Phys. Rev. Lett.*, *107*, 135701, doi:10.1103/PhysRevLett.107.135701.
- Zhang, Y.-W., X. Sun, R. Si, L.-P. You, and C.-H. Yan (2005a), Single-crystalline and monodisperse LaF₃ triangular nanoplates from a single-source precursor., *Journal of the American Chemical Society*, *127*(10), 3260–1, doi:10.1021/ja042801y.
- Zhang, Z., A. S. Keys, T. Chen, and S. C. Glotzer (2005b), Self-assembly of patchy particles into diamond structures through molecular mimicry., *Langmuir : the ACS journal of surfaces and colloids*, *21*(25), 11,547–51, doi:10.1021/la0513611.
- Zhao, K., R. Bruinsma, and T. G. Mason (2011), Entropic crystal-crystal transitions of Brownian squares., *Proceedings of the National Academy of Sciences of the United States of America*, *108*(7), 2684–7, doi:10.1073/pnas.1014942108.
- Zhao, K., R. Bruinsma, and T. G. Mason (2012), Local chiral symmetry breaking in triatic liquid crystals, *Nature Communications*, *3*, 801.
- Zhou, B., Y. Ji, Y.-F. Yang, X.-H. Li, and J.-J. Zhu (2008), Rapid Microwave-Assisted Synthesis of Single-Crystalline Sb₂Te₃ Hexagonal Nanoplates, *Crystal Growth & Design*, *8*(12), 4394–4397, doi:10.1021/cg7011815.